Evaluation of a new model of aeolian transport in the presence of vegetation

Junran Li,[1,2] Gregory S. Okin,[2] Jeffrey E. Herrick,[1] Jayne Belnap,[3] Mark E. Miller,[4] Kimberly Vest,[5] and Amy E. Draut[6]

Received 13 February 2012; revised 30 January 2013; accepted 5 February 2013; published 26 March 2013.

[1] Aeolian transport is an important characteristic of many arid and semiarid regions worldwide that affects dust emission and ecosystem processes. The purpose of this paper is to evaluate a recent model of aeolian transport in the presence of vegetation. This approach differs from previous models by accounting for how vegetation affects the distribution of shear velocity on the surface rather than merely calculating the average effect of vegetation on surface shear velocity or simply using empirical relationships. Vegetation, soil, and meteorological data at 65 field sites with measurements of horizontal aeolian flux were collected from the Western United States. Measured fluxes were tested against modeled values to evaluate model performance, to obtain a set of optimum model parameters, and to estimate the uncertainty in these parameters. The same field data were used to model horizontal aeolian flux using three other schemes. Our results show that the model can predict horizontal aeolian flux with an approximate relative error of 2.1 and that further empirical corrections can reduce the approximate relative error to 1.0. The level of error is within what would be expected given uncertainties in threshold shear velocity and wind speed at our sites. The model outperforms the alternative schemes both in terms of approximate relative error and the number of sites at which threshold shear velocity was exceeded. These results lend support to an understanding of the physics of aeolian transport in which (1) vegetation's impact on transport is dependent upon the distribution of vegetation rather than merely its average lateral cover and (2) vegetation impacts surface shear stress locally by depressing it in the immediate lee of plants rather than by changing the bulk surface's threshold shear velocity. Our results also suggest that threshold shear velocity is exceeded more than might be estimated by single measurements of threshold shear stress and roughness length commonly associated with vegetated surfaces, highlighting the variation of threshold shear velocity with space and time in real landscapes.

Citation: Li, J., G. S. Okin, J. E. Herrick, J. Belnap, M. E. Miller, K. Vest, and A. E. Draut (2013), Evaluation of a new model of aeolian transport in the presence of vegetation, *J. Geophys. Res. Earth Surf.*, *118*, 288–306, doi:10.1002/jgrf.20040.

Notation

- a equation (1) fitting constant, m^{-2}
- A constant present in equations for $Q^{u_*}_{x/h}$ of the form $A\rho/gu_*{}^X$ (Table 3), $m^{3-X}\,s^{X-3}$
- A_B average area of a single vegetation element (plant) projected onto the ground (i.e., basal area), m^2
- A_P average area of a single vegetation element (plant) projected onto a plane perpendicular to the ground (i.e., profile area), m^2
- b equation (1) fitting constant, m^{-1}
- β ratio of drag coefficient for vegetation to drag coefficient for ground ($\beta = 202$) [*Shao*, 2008, p. 307]

All Supporting Information may be found in the online version of this article.

[1]USDA-ARS Jornada Experimental Range, New Mexico State University, Las Cruces, New Mexico, USA.
[2]Department of Geography, University of California, Los Angeles, California, USA.
[3]U.S. Geological Survey, Southwest Biological Science Center, Moab, Utah, USA.
[4]National Park Service, Canyonlands National Park, Moab, Utah, USA.
[5]University of Maryland Center for Environmental Sciences, Appalachian Lab, Frostburg, Maryland, USA.
[6]U.S. Geological Survey, Pacific Science Center, Santa Cruz, California, USA.

Corresponding author: G. S. Okin, Department of Geography, University of California, Los Angeles, CA 90095, USA. (okin@ucla.edu)

2169-9003/13/10.1002/jgrf.20040

c equation (1) fitting constant, $g\,m^{-2}\,s^{-1}$
C e-folding distance for the recovery of u_{*s} in the lee of a plant as it approaches u_*
δ constant, $\delta = 0$ when $u_* < u_{*t}$ and $\delta = 1$ when $u_* > u_{*t}$
$\bar{D}$ average plant diameter, m
D_P particle size diameter, used in MAR model, m
EF erodible fraction used in RWEQ model
ε_r approximate relative error of model estimates
f_{eff} drag partition coefficient [*Marticorena et al.*, 1997b]
f_{eff,z_1} drag partition coefficient induced by soil surface roughness [*Marticorena et al.*, 1997b]
f_{eff,z_2} drag partition coefficient induced by soil vegetation [*Marticorena et al.*, 1997b]
F_g fraction of the ground that is covered by plants
g acceleration due to gravity, $m\,s^{-2}$
h plant height, measured as Frisbee™ drop height, m
K Von Karman's constant, 0.4
K' soil roughness factor used in RWEQ model
$\bar{L}$ average size of unvegetated gaps between plants, m
λ lateral cover
m empirical parameter [*Raupach et al.*, 1993]
n number of field sites
$P_d(x/h)$ probability that a point on the landscape is distance from the nearest upwind plant measured as x/h
P_U probability distribution of wind speeds, U, during measurement period
P_{u_*} probability distribution of wind shear velocity, u_*, during measurement period
$Q_{t,\text{act}}$ field-estimated horizontal flux, $g\,m^{-1}\,d^{-1}$
$Q_{t,\text{corr}}$ empirically corrected model-estimated horizontal flux, $g\,m^{-1}\,d^{-1}$
$Q_{t,\text{pred}}$ model-estimated horizontal flux, $g\,m^{-1}\,d^{-1}$
$Q_t^{u_*}$ model-estimated horizontal flux at shear velocity, u_*, $g\,m^{-1}\,d^{-1}$
$Q_{x/h}^{u_*}$ horizontal flux at shear velocity u_* and distance from nearest upwind plant measured as x/h, $g\,m^{-1}\,d^{-1}$
$q(z)$ time-averaged horizontal flux density at height z above the surface, measured with a BSNE, $g\,m^{-2}\,d^{-1}$
ρ density of air, $g\,m^{-3}$
$RMSEL$ root mean squared error of the logs of horizontal flux
σ ratio of roughness-element basal area to frontal area, A_B/A_P
SCF soil crust factor used in RWEQ model
SD soil snow cover correction in the RWEQ model
SLR_C soil loss ratio correcting for the growing plant canopy cover in the RWEQ model
SLR_F soil loss ratio correcting for flat residue in the RWEQ model
SLR_S soil loss ratio correcting for the plant silhouette in the RWEQ model
SW soil wetness correction in the RWEQ model
U_t threshold wind speed at 2 m in the RWEQ model, $m\,s^{-1}$
U_z horizontal wind speed at height z, $m\,s^{-1}$
u_* shear velocity of the wind, $m\,s^{-1}$
u_{*s} shear velocity in the lee of a plant (as a function of x/h), $m\,s^{-1}$
$\left(\frac{u_{*s}}{u_*}\right)_{x=0}$ ratio of shear velocity in the immediate lee of a plant ($x = 0$) to shear velocity as estimated with the Law of the Wall
u_{*t} threshold shear velocity of the soil, $m\,s^{-1}$
$u_{*\text{tv}}$ threshold shear velocity of the surface in the presence of vegetation [*Marticorena et al.*, 1997b; *Shao*, 2008], $m\,s^{-1}$
$\bar{W}$ average plant width along a transect, equal to $\pi/4\ \bar{D}$ for circular plants, m
WF weather factor in RWEQ model, $g\,m^{-1}\,d^{-1}$
x distance to nearest upwind plant, m
x/h distance to nearest upwind plant measured as distance, x, scaled by plant height, h
X_1 reciprocal of distance between soil roughness elements [*Marticorena et al.*, 1997b], set to 0.1 m
X_2 one-third of the distance between plants [*Marticorena et al.*, 1997b], m
Y regression-derived value of Q_t in equation (10), $g\,m^{-1}\,d^{-1}$
z height above ground surface, m
z_o aerodynamic roughness length, m
$z_{o,1}$ aerodynamic roughness length induced by soil surface [*Marticorena et al.*, 1997b], m
$z_{o,2}$ aerodynamic roughness length induced by [*Marticorena et al.*, 1997b], m
z_{os} aerodynamic roughness length for a smooth surface, 10^{-5} m [*Marticorena et al.*, 1997b]

1. Introduction

[2] Aeolian transport is a fundamental process in the world's drylands, and it has direct impacts on climate, ecosystem dynamics, soil biogeochemical cycling, snow accumulation and melt, precipitation runoff, and public safety/health [*Sokolik and Toon*, 1996; *Li et al.*, 2007, Li *et al.*, 2008, *Reynolds et al.*, 2001; *Painter et al.*, 2007, *Painter et al.*, 2010; *Griffin et al.*, 2001]. Most aeolian transport occurs in arid and semiarid lands that cover nearly 40% of the land surface [*Reynolds and Stafford Smith*, 2002]. A report by *Seager et al.* [2007] predicts reduced soil moisture and increasingly arid conditions in the next decades over large areas of the arid Southwest United States and other studies have predicted aridification elsewhere [e.g., *Thomas et al.*, 2005]. The ability to estimate aeolian activity from process-based models is important for predicting future changes in aeolian activity given expected changes in climate, vegetation, and land use in the world's drylands. This is particularly true given the difficulty of measuring aeolian transport at the large scales that characterize the world's rangelands (e.g., greater than 100s of square kilometers), which is the most common form of land use in drylands.

[3] Aeolian transport is strongly affected by nonerodible roughness elements such as immobile clasts and vegetation [*Lancaster and Baas*, 1998; *Tegen et al.*, 2002; *Gillies et al.*, 2006], which absorb a portion of the shear stress exerted by the wind. On a vegetated surface, the amount of roughness encountered by the wind has been most widely

quantified by an index of "lateral cover", λ, which is defined as the average frontal area of plants projected onto a plane perpendicular to both the ground surface and direction of the wind multiplied by their number density. Since *Marshall* [1971], lateral cover has been the primary parameter representing the amount of vegetation in shear stress partitioning models [e.g., *Marticorena et al*., 1997b; *Raupach*, 1992] and subsequent models for wind erosion and dust emission on vegetated surfaces [e.g., *Marticorena and Bergametti*, 1995; *Mahowald et al*., 2002; *Zender et al*., 2003]. Application of the *Raupach* [1992] shear stress partitioning model does lead to shear stress ratios (i.e., the ratio of shear stress on the soil to the total shear stress) that are consistent with experimental results [*King et al*., 2005]. However, this model estimates threshold shear velocities in the presence of vegetation [*Raupach et al*., 1993] that are too high to produce horizontal flux given normal erosive winds when the lateral cover is greater than about 0.1 [*Okin*, 2008]. Field experiments, including those of *Lancaster and Baas* [1998] in Owens Valley, *Li et al*. [2007] in the Chihuahuan Desert (Figure 1), and *Belnap et al*. [2009] on the Colorado Plateau, in contrast, show that significant flux occurs even at relatively high lateral cover values.

[4] *Okin* [2008] pointed out that the discrepancy between model-predicted aeolian transport using lateral cover [e.g., *Marticorena et al*., 1997b; *Raupach*, 1992] and field-observed fluxes potentially results from the requirement that threshold shear velocity be the same everywhere. Conceptually, this is due to the fact that lateral cover only provides information on the density of vegetation but says nothing about how that vegetation is distributed and therefore the model can provide only estimates of the surface stress averaged over the exposed soil area. This issue was identified originally by *Raupach et al*. [1993], who introduced an empirical parameter (the *m* parameter) that was intended to adjust the lateral cover so that surface stress would be given by the maximum surface stress on the exposed soil area rather than the surface stress averaged over the exposed soil area.

[5] Field observations have shown that horizontal sediment flux can be strongly affected by the spatial distribution of vegetation [*Okin and Gillette*, 2001; *Gillette et al*., 2006]. Recently, *Okin* [2008] developed a new aeolian transport model using the distribution of erodible gaps between plants to characterize shear stress partitioning and distribution of shear stress at the soil surface. This new model provides very good estimates of shear stress ratios compared to laboratory and field experiments. In addition, it predicts horizontal flux in vegetation with relatively high densities ($\lambda > 0.1$), consistent with field observations (e.g., Figure 1). It does so by not requiring the flux to occur at all points in the landscape at the same time; winds in some areas protected by vegetation can be below threshold while winds in more exposed area can be above threshold. The physics represented by this model are consistent with a host of measurements and independent model results. For example, the model represents shear stress in the lee of plants in a way consistent with the field measurements of *Bradley and Mulhearn* [1983], the wind tunnel measurements of *Minvielle et al*. [2003] and wind speed distributions modeled using a fluid flow model [*Bowker et al*., 2006].

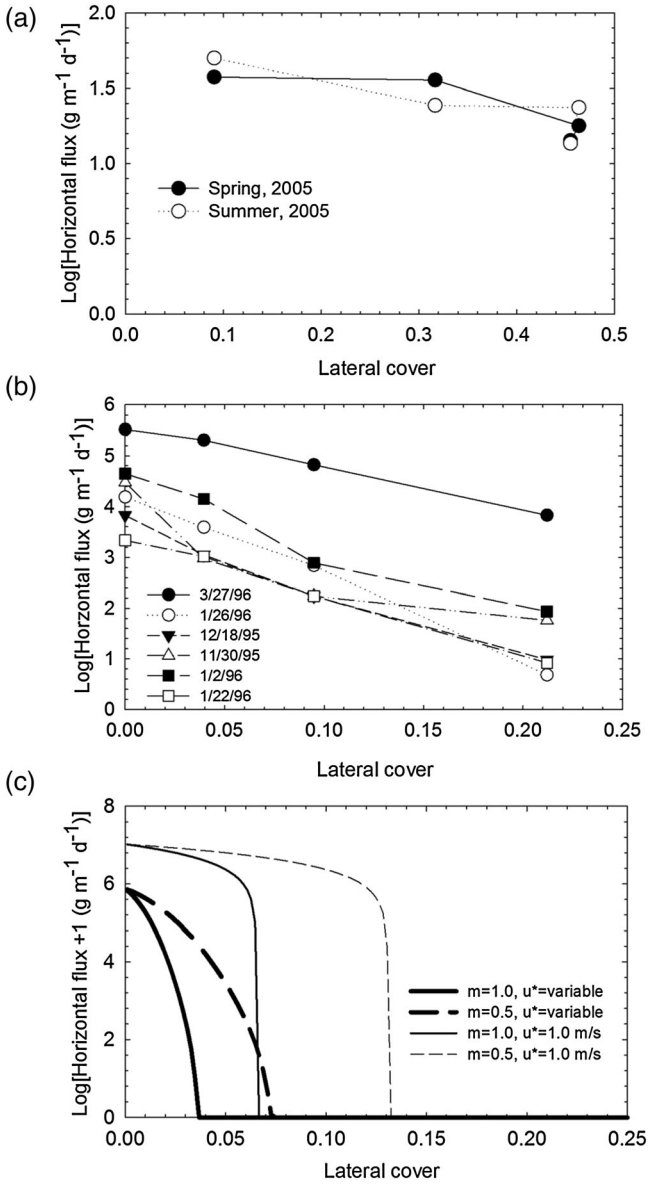

Figure 1. Horizontal flux versus lateral cover for (a and b) field experiments and (c) model prediction. Figure 1a: data from individual storms from Owens Dry Lake [*Lancaster and Baas*, 1998]; Figure 1b: data from two seasons in the Chihuahuan Desert [*Li et al*., 2007]; and Figure 1c: estimates of total horizontal flux using the shear stress partitioning model of *Raupach et al*. [1993] and the flux equation of *Shao and Raupach* [1992] using two values of *m*, 0.5 and 1.0. Light lines are horizontal flux estimated at constant shear velocity ($1.0\,\mathrm{m\,s^{-1}}$) and heavy lines are flux estimates for actual wind speed records of the Jornada Experimental Range in New Mexico from 1997 to 2001. Figure redrawn from *Okin* [2008].

[6] The purpose of this paper is to evaluate the *Okin* [2008] model of aeolian transport in the presence of vegetation (hereafter referred to as OK) and to estimate the best values for its parameters. Our strategy was to collect vegetation, soil, and meteorological data for wind erodible sites where aeolian transport was actively monitored at the

time of the research. Measured aeolian fluxes were then tested against modeled values to evaluate the model performance, to obtain a set of optimum model parameters, and to estimate the uncertainty in these parameters. The same field data were used to model horizontal flux using other schemes, including those of the Revised Wind Erosion Equation (RWEQ) [*Fryrear et al*., 1998], *Marticorena et al*. [1997b], and *Shao* [2008 p. 307], slightly modified so that their treatment of vegetation can be directly compared to that of the OK model using the same dataset. We wish to determine whether this model can be used to predict horizontal aeolian transport in real, structurally complex vegetation. More critically, we wish to determine whether aeolian transport can occur in some exposed areas and not in other more protected areas (i.e., rather than requiring the entire landscape to have a single threshold), which may provide a more realistic picture of the physics of aeolian transport in vegetated landscapes.

2. Methods and Data

2.1. Description of the Sites

[7] Our field sites were located in Utah, New Mexico, and California (Table 1). These sites represent all of the known actively monitored wind erosion sites in the western United States at the time this project was conducted. None of these sites were established for the purpose of conducting model evaluation. Because sites were established for other reasons, some measurements that would have been helpful for this study, especially meteorological observations near flux measurements, were not available and alternative, nearby observations had to be used instead. Evaluation of the impact of the uncertainty in meteorological observations is discussed below.

[8] At each site, horizontal aeolian flux was monitored by a set of samplers ("stems") utilizing Big Spring Number Eight (BSNE) aeolian sediment traps [*Fryrear*, 1986]. BSNEs at each site were located in an open and topographically flat area, without large shrubs in the immediate upwind or downwind area. The traps were able to move freely with the direction of the wind so that the inlet always faced into the wind. A total of 65 BSNE stems was found that met the following criteria: (1) each BSNE stem was equipped with at least three traps, and (2) the mass of windblown sediment collected in the BSNE traps monotonically decreased with the increase of trap height. The latter criterion ensures that the sediment in traps is not dominated by nonlocal sources [*Bergametti and Gillette*, 2010]. The heights of the arithmetic center of the openings of the BSNE traps were recorded. The lowest traps were located ~0.1-0.15 m above ground surface and the top traps were mounted at about 1 m high. The deployment periods for the BSNE stems varied at different sites (Table 1), and windblown sediments were collected at the end of the experimental period.

[9] For the Fivemile Mountain sites in Utah, shrubs were either removed or thinned by different mechanical treatments that varied in their effects on soil stability, vegetation structure, and the amount and distribution of residual woody debris. BSNE stems on the Clear Spot Flat sites were mostly located on lands burned by a severe wildfire in July 2007 and subsequently seeded using mechanical techniques that impacted soil erodibility (more detail can be found in

Table 1. Locations and Environmental Characteristics of the Study Sites

	Moab, UT	Fivemile Mountain, UT	Clear Spot Flat, UT	Jornada Experimental Range, NM	Owens Valley, CA
Plant community	Shrubby grassland	Shrubland	Shrubland	Shrubby grassland	Shrubby grassland
Dominant species	*Sarcobatus vermiculatus*, *Atriplex canescens*, *Stipa comata*	*Artemisia tridentata*	*At. confertifolia*, *Halogeton glomeratus*, *Salsola tragus*	*Prosopis glandulosa*, *Larrea tridentate*, *Bouteloua eriopoda*	*Sar. vermiculatus*, *At. torreyi*, *Distichlis spicata*
Treatment	—	Mech. treated	Burned and Mech. treated	Shrub removal[b]	—
Annual rainfall (mm)	230	340	227	247	128
Elevation (m)	1227	1515	1524	1250	1264
Soil texture[d]	SaL	SaL, SiL	SaL, SiL, L	Sa	LSa, SaL
Roughness elements	Vegetation,soil crust	Vegetation, woody debris	Vegetation, woody debris	Vegetation	Vegetation, rocks
Wind data	CLIM-MET[a]	On-site	On-site	On-site	On-site, WRCC[c]
Number of BSNEs	25	10	2	15	13
Duration of BSNE deployment	Mar–Jul 2009	Mar–Jul 2009	Mar–Jun 2009	Mar–Jun 2009	May–Sept 2009

[a]CLIM-MET-Southwest Climate Impact Meteorological Stations, operated by the U.S. Geological Survey Geology and Environmental Change Science Center.
[b]Shrub removal was conducted in part of the Jornada sites, see details in *Li et al.* [2007].
[c]WRCC-Western Regional Climate Center, operated by the Desert Research Institute.
[d]SaL = sandy loam, SiL = silt loam, L = loam, Sa = sand, and LSa = loamy sand.

Miller et al. [2012]). At the Jornada Experimental Range (JER), BSNE stems were located in a grassland with various levels of vegetation removal [*Li et al*., 2007]. The reduced vegetation cover at the JER sites has been maintained since their establishment in summer 2004.

2.2. Additional In Situ Data Collection and Processing

[10] At each BSNE stem site, fractional (foliar) vegetation cover and distribution of unvegetated gaps were measured using a modified version of Standard NRCS National Resources Inventory Methods [*Herrick et al*., 2005]. At non-JER sites, all measurements were conducted along three 50-m transects oriented at 100°, 220°, and 340° from due north and were set up beginning 5 m from the BSNE stems. At the JER sites, measurements were conducted along three 50-m transects oriented in the direction of the prevailing wind. For intercanopy gap measurements, only perennials and persistent woody debris from dead trees/shrubs were counted as gap stoppers and a minimum gap size was set as 20 cm. For each span of canopy between two gaps, canopy heights were determined by measuring the height of the center of a Frisbee™ (186 g, with a hole in the center) dropped along a meter stick from a height of 10 cm above the maximum canopy height. This empirical approach was used to approximate the effect of wind shear stress bending the top of the plants and to eliminate the effect of small/thin leaves or stems that may protrude significantly from the main canopy but which probably have little impact on airflow. A distribution of scaled gap sizes was calculated as the ratio between a gap and the adjacent plant canopy height (Frisbee dropped height) for all gaps and canopies along each of the transects (Figure 2a). Subsequently, a histogram of the gap size, scaled by adjacent plant height, was constructed (Figure 2b).

[11] Threshold shear velocity (u_{*t}) for unvegetated soils (Table 2) (i.e., for the soil itself rather than the vegetated surface as a whole) was estimated using a method developed by *Li et al*. [2010]. In this method, u_{*t} was quantitatively related with the resistance of the soil surface to disturbances created by a penetrometer and projectile shot by an air gun at the soil. Briefly, at each BSNE stem, a total of 15 repeated air gun and penetrometer measurements were

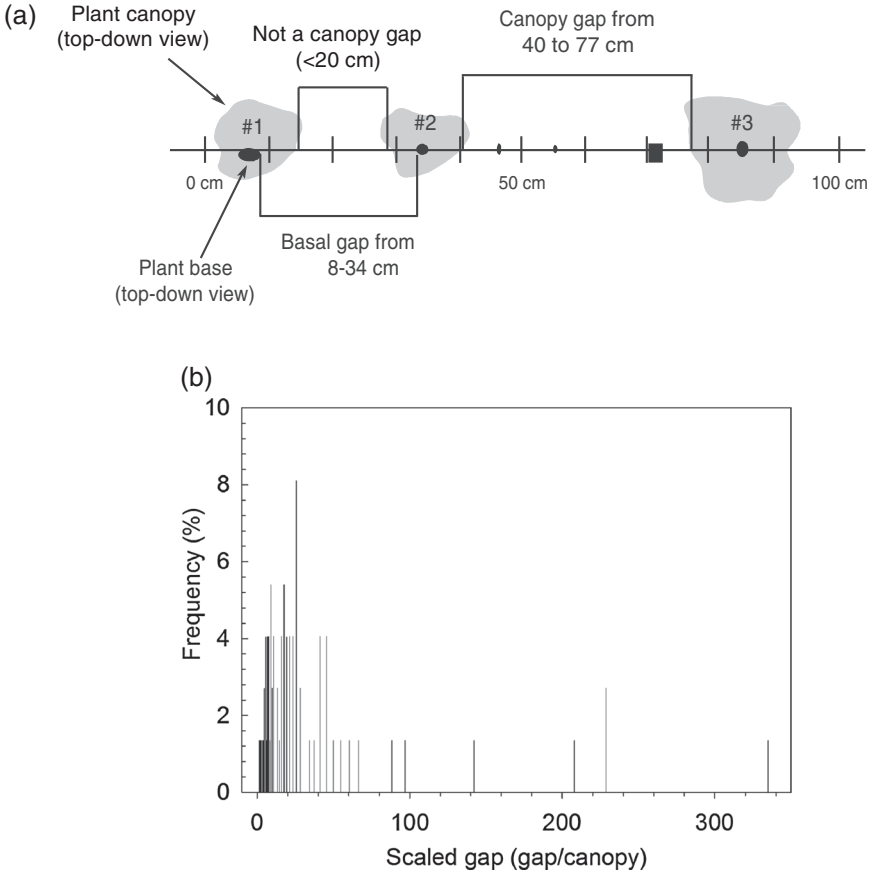

Figure 2. (a) Illustration of unvegetated gap and plant canopy measurement in the field, with three plants (indicated by #1–#3) and one effective gap in a 1-m section of a plant transect. In this section, the only canopy gap has the size of $77 - 40 = 37$ cm, and assuming the plant immediate follow the gap (#3) has the canopy height of 10 cm, the scaled gap would be $37/10 = 3.7$. In the field, a distribution of the scaled gap was calculated for all gaps and canopy heights along each of the 50-m long transects. Revised from *Herrick et al*. [2005]. (b) An example of a histogram of the scaled gap size measured in Moab, Utah, constructed based on the size of a gap and the height of an adjacent plant canopy for all gaps and canopies along three 50-m transects.

Table 2. The Characteristics of Vegetation, Wind, and Estimated Threshold Shear Velocity for Unvegetated Soils

Parameters	Moab, UT	Fivemile Mountain, UT	Clear Spot Flat, UT	Jornada Experimental Range, NM	Owens Valley, CA
Fractional plant cover (F_g, %)	~0–58	9–33	~0–36	11–27	29–78
Max gap (m)	>50	8	22	21	34
Median gap (m)	2.35	0.59	2.28	1.83	1.13
Max gap/canopy height	2212	446	2179	994	752
Median gap/canopy height	40	9	35	22	12
Max wind speed ($m\,s^{-1}$)	12.0[a]	13.9[a]	15.2[a]	18.3[b]	26.4[b]
Threshold shear velocity (u_{*t}, $m\,s^{-1}$)	0.26–0.97	0.31–0.54	0.26–1.04	0.19–0.54	0.36–0.91

[a]At the height of 3 m.
[b]At the height of 10 m.

conducted along each transect starting from 5 m with an interval of 10 m. Both air gun and penetrometer were applied at 45° to the soil surface, and the readings from the penetrometer and sizes of the surface soil disturbance (length × width) created by the air gun were recorded. Average values were used to evaluate a regression equation to estimate u_{*t}.

[12] Horizontal wind speed (U) data were obtained from on-site meteorological towers or wind towers located nearby and operated by other organizations (Table 1). The interval of the wind speed records varied from 5 min to 1 h. Wind data used in modeling were compiled for each horizontal flux estimate for the same period of sample collection.

[13] Total horizontal mass flux from the BSNEs ($Q_{t,\mathrm{act}}$, expressed in units of mass per unit distance perpendicular to both the wind and the ground per unit time, $M\,L^{-1}\,t^{-1}$) was calculated based on the weight of sediments collected in each BSNE trap and their deployment time by using the method described in *Li et al*. [2007]. The mass of sediments collected in the BSNE traps was divided by the inlet area of the trap ($1.05 \times 10^{-3}\,m^2$) and the time of the collection to obtain the time-averaged horizontal mass flux density $q(z)$ in $g\,m^{-2}\,d^{-1}$, where z is the height of the arithmetic center of the inlet above the ground (m). Values of $q(z)$ were fitted to an empirical formula [*Shao and Raupach*, 1992]:

$$q(z) = c\mathrm{Exp}\left(ah^2 + bh\right) \tag{1}$$

[14] where a, b, and c are fitting constants. The values for total horizontal flux $Q_{t,\mathrm{act}}$, in $g\,m^{-1}\,d^{-1}$, were calculated by

$$Q_{t,\mathrm{act}} = \int_{0m}^{1m} q(z)dz \tag{2}$$

[15] The maximum height of integration was set to 1 m because only a small percentage of the flux (generally less than 10%) occurs at heights >1 m [*Li et al*., 2007].

2.3. Description of the Model

[16] The details of the wind erosion model have been described by *Okin* [2008]. In brief, prediction of the horizontal aeolian flux $Q_t^{u_*}$ for a specific wind shear velocity, u_* ($m\,s^{-1}$), is achieved by modeling the distribution of gaps downwind of plant canopies as

$$Q_t^{u_*} = \left(1 - F_g\right)\sum_{x/h} Q_{x/h}^{u_*} P_d(x/h) \tag{3}$$

where F_g is the ground fraction that is covered by vegetation, x is a distance from the nearest upwind plant (m), h is the height of that plant (m), $Q_{x/h}^{u_*}$ is the horizontal flux for a point x/h away from the nearest upwind plant at the shear velocity, u_*, and $P_d(x/h)$ is the probability that any point in the landscape is a certain distance from the nearest upwind plant expressed in units of height of that plant. The overall horizontal flux ($Q_{t,\mathrm{pred}}$) for all wind speeds is calculated by

$$Q_{t,\mathrm{pred}} = \sum_{u_*} P_{u_*} Q_t^{u_*} \tag{4}$$

in which P_{u_*} is the probability distribution of wind shear velocity, u_*, during measurement period.

[17] In the OK model as originally published, horizontal flux at a certain point, $Q_{x/h}^{u_*}$, is calculated using the formulation of *Owen* [1964] and redefined by *Shao et al*. [1993] and *Gillette and Chen* [2001]:

$$Q_{x/h}^{u_*} = A\frac{\rho}{g}u_*\left({u_*}^2 - {u_{*t}}^2\right)\delta \tag{5}$$

where A is a dimensionless constant that may vary between 0 and 1, ρ is the density of air ($g\,m^{-3}$), g is the acceleration due to gravity ($m\,s^{-2}$), u_{*t} is the threshold shear velocity of the unvegetated soil ($m\,s^{-1}$), and δ is a constant with $\delta = 0$ when $u_* < u_{*t}$ and $\delta = 1$ when $u_* > u_{*t}$. In the OK model and all the other wind erosion models evaluated in this paper, the units of model simulated horizontal aeolian fluxes (Q) were converted from $g\,m^{-1}\,s^{-1}$ to $g\,m^{-1}\,d^{-1}$. Although not standard SI units, we use $g\,m^{-1}\,d^{-1}$ because we believe that this unit provides a better relation to the temporal scale at which aeolian flux was measured (days to months).

[18] The OK model assumes each plant is associated with a reduced shear stress wake zone and this zone of reduced shear stress is described by an exponential curve:

$$u_{*s} = u_*\left(\left(\frac{u_{*s}}{u_*}\right)_{x=0} + \left(1 - \left(\frac{u_{*s}}{u_*}\right)_{x=0}\right)\left(1 - e^{-C/(x/h)}\right)\right) \tag{6}$$

where u_{*s} is the shear velocity downwind of a plant, $\left(\frac{u_{*s}}{u_*}\right)_{x=0}$ is the value of u_{*s}/u_* in the immediate lee of a plant, and C is the e-folding distance for the recovery of the shear velocity in the lee of plants (that is, C is the exponential constant that describes the rate, in units of plant height, h,

at which the shear velocity, u_{*s}, recovers to the value it would have in the absence of vegetation, u_*). The physical meaning of these parameters is summarized in Table 3.

[19] In the model, u_* is related to the mean wind speed, U, at height z (m) by a rearranged form of Law of the Wall:

$$u_* = {}^{UK}\Big/_{\ln\left(\frac{z}{z_o}\right)} \tag{7}$$

where K is von Karman's constant ($K = 0.4$), and z_o is aerodynamic roughness length (m).

[20] At the scale of many wind erosion models, the roughness length (z_o) varies over heterogeneous landscapes as it is related to both plant lateral cover and canopy height [e.g., *Marticorena et al*., 1997a]. In the OK model, z_o is set as a constant for all sites. This allowed us to treat z_o as a fitting parameter in our model validation and meant that z_o would not have to be estimated at each field site. Other model input parameters, including A, C, and $\left(\frac{u_{*s}}{u_*}\right)_{x=0}$, were also treated as constant for the purpose of the model validation. In the OK model, the impact of the shrub structure is accounted for mostly in the $\left(\frac{u_{*s}}{u_*}\right)_{x=0}$ parameter. In reality, to some extent, the vegetation structure will impact shear stress partitioning and therefore $\left(\frac{u_{*s}}{u_*}\right)_{x=0}$, but there is in fact a remarkable degree of overlap in shear stress partitioning ratio amongst solid and porous objects [*King et al*., 2005]. When examining all available shear stress partitioning ratio in light of the OK model, there was no clear value of $\left(\frac{u_{*s}}{u_*}\right)_{x=0}$ that separated solid from porous objects, although there was a slight bias toward higher values of $\left(\frac{u_{*s}}{u_*}\right)_{x=0}$ for porous objects. In light of these observations, it is unclear how much $\left(\frac{u_{*s}}{u_*}\right)_{x=0}$ would vary amongst porous objects. In short, there is no compelling reason based on existing data to treat $\left(\frac{u_{*s}}{u_*}\right)_{x=0}$ as anything but a bulk constant. The parameter C, too, may vary with shrub structure or porosity, but in the absence of experimental or theoretical guidance on this and for the purpose of parsimony, it has been treated as a constant.

[21] In recognition of the fact that z_o does change with vegetation density, a modified version of the *Okin* [2008] model (hereafter called the "modified *Okin* [2008] model" or MOK) was also implemented. In this modified model, z_o was allowed to vary as a function of lateral cover, using the approach of *Marticorena et al*. [1997b] as presented by *Shao* [2008, p. 318], with additional modifications. First, z_o was calculated using

$$z_o = \begin{cases} (0.48\lambda + 0.001)h & \lambda < 0.11 \\ 0.0538h & \lambda \geq 0.11 \end{cases} \tag{8}$$

Okin [2008] showed that lateral cover, λ, was related to average gap size by

$$\lambda = \frac{A_P \bar{W}}{A_B\left(\bar{L} + \bar{W}\right)} \tag{9}$$

where A_P is the profile area of a plant, A_B is the basal area of a plant, $\bar{L}$ is the average size of unvegetated gaps between plants, and $\bar{W}$ is the average width of a plant along a transect (equal to $\pi/4$ of the plant diameter, $\bar{D}$, for circular plants). The fractional cover of a plant, F_g, is given, in these terms, by

$$F_g = \frac{\bar{W}}{\bar{L} + \bar{V}} \tag{10}$$

[22] Assuming cylindrical geometry (i.e., $A_B = \pi/4\bar{D}^2$ and $A_P = \bar{D}h$), it can be shown that

$$\lambda = \left(1 - F_g\right)\frac{h}{\bar{L}} \tag{11}$$

[23] Initial tests using equation (8) for aerodynamic roughness length alone showed that for field sites without vegetation cover, the model produced no flux because z_o was too low and the resulting u_* never exceeded u_{*t}. This is in direct contradiction with our field measurements; bare sites did produce significant amount of horizontal flux. So, a modified aerodynamic roughness length, z'_o, was used in MOK instead of z_o calculated from equation (8). Specifically, a linear relationship was applied that adjusted all roughness values:

$$z'_o = z_{o,\min} + z_o\left(\frac{z_{o,\text{tie}} - z_{o,\min}}{z_{o,\text{tie}}}\right) \tag{12}$$

where $z_{o,\min}$ is the minimum value for z'_0 and was set to 0.01 m and $z_{o,\text{tie}}$ was set to 0.1 m.

[24] In this study, several different horizontal flux equations were tried in place of equation (5) in both the OK and MOK models. Over the past few decades, many experimental and numerical studies have investigated the variation of horizontal mass flux with shear velocity. These studies have led to different equations but predominantly with the form that $Q_{t,\text{pred}}$ scales with approximately the third power of the shear velocity. We tested the model performance in combination

Table 3. Description of the Important Input Parameters Used in the Model

Parameters	Physical Meaning	Range/Value in Literature	Relevant Literature
z_o	Roughness length, m	10^{-7}–10^{-1} m	*Marticorena et al*. [1997a]; *Gillette et al*. [2006]
A	Constant with variable units[a]	0 to ~1	*Gillette and Chen* [2001]
C	*e*-folding distance for recovery of the shear stress in the lee of plants, dimensionless	4.8–10	*Minvielle et al*. [2003], *Bradley and Mulhearn* [1983]
$\left(\frac{u_{*s}}{u_*}\right)_{x=0}$	Shear velocity ratio in the immediate lee of a plant, dimensionless	0.0–0.32	*Okin* [2008], *Bradley and Mulhearn* [1983]

[a]Units of A depend on the form of the flux equation in Table 4: $u_*^4 = \text{s m}^{-1}$, $u_*^3 = $ dimensionless, $u_*^2 = \text{m s}^{-1}$.

with the horizontal mass flux equations in Table 4, and since there is some question in the literature concerning the exponent of the shear velocity in mass flux equation, equations from the second to the fourth power were used. For the OK model, the best equation was identified, together with the set of model parameters: z_o, A, C, and $\left(\frac{u_{ss}}{u_*}\right)_{x=0}$. For the MOK model, the best equation was also identified, together with the set of model parameters: A, C, and $\left(\frac{u_{ss}}{u_*}\right)_{x=0}$.

2.4. Parameter Estimation and Cross-Validation

[25] An algorithm aimed at finding the global minimum error was employed. Random values of Log[A], C, $\left(\frac{u_{ss}}{u_*}\right)_{x=0}$, and Log[$z_o$] (for OK) were chosen from uniform distributions bounded by physically reasonable values of each of the parameters (Table 5). Predicted values of $Q_{t,\mathrm{pred}}$ were calculated for all BSNE stems used in the minimization, and the root mean squared error of the logs (*RMSEL*) was calculated as

$$RMSEL = \left(\frac{1}{N}\sum_{N}\left(\mathrm{Log}\left(Q_{t,\mathrm{pred}}\right) - \mathrm{Log}\left(Q_{t,\mathrm{act}}\right)\right)^2\right)^{1/2} \quad (13)$$

where $Q_{t,\mathrm{pred}}$ is the predicted value of horizontal flux using the randomly selected parameter values, $Q_{t,\mathrm{act}}$ is the value of horizontal flux estimated from the BSNE stems, and N is the number of measurements used in the minimization. *RMSEL* is dimensionless because the difference between the logs of two quantities, as in equation 13, is equal to the log of their ratio. A small constant ($\ll$ minimum ($Q_{t,\mathrm{act}}$)) was added to both $Q_{t,\mathrm{pred}}$ and $Q_{t,\mathrm{act}}$ to prevent values of negative infinity if either equals zero. This was done 1000 times and the set of parameters that yielded the lowest *RMSEL* was chosen as the best-fit set of parameters.

[26] This iterative process was conducted 65 times. Each time, 64 sites were used in the error minimization ($N = 64$), while one was left out (i.e., each site was left out once). The final *RMSEL* was calculated using equation (13) but substituting the predicted values for the omitted site as $Q_{t,\mathrm{pred}}$ and the actual horizontal flux values of the omitted site as $Q_{t,\mathrm{act}}$. This leave-one-out cross-validation analysis was conducted to provide mean estimates of key model parameters and was done for every flux equation in Table 4.

Table 5. Bounding Values of Uniform Distributions Used for Random Selection of Values for Error Minimization

Parameter	Minimum Value	Maximum Value
Log[A]	−6	−3
C	4.8	9.0
$(\frac{u_{ss}}{u_*})_{x=0}$	0.0	0.4
Log[z_o]	−1.0	0.5

[27] Error estimation and model comparison are further discussed below.

2.5. Empirical Model Improvement by Stepwise Regression of Residuals

[28] Although the main goal of this study was to validate the process-based OK, additional steps were taken after the best-fit flux equation and model parameters were determined. From this best model, a stepwise regression was conducted on residuals in log space:

$$residual = \mathrm{Log}\left(Q_{t,\mathrm{act}}\right) - \mathrm{Log}\left(Q_{t,\mathrm{pred}}\right) \quad (14)$$

[29] In this process, the field-derived parameter that had the highest absolute correlation (i.e., $|r|$) with $Q_{t,\mathrm{act}}$ was determined and residuals were regressed against this parameter. A correction was then calculated based on the following regression:

$$\mathrm{Log}\left(Q_{t,\mathrm{corr}}\right) = \mathrm{Log}\left(Q_{t,\mathrm{pred}}\right) + Y \quad (15)$$

where Log($Q_{t,\mathrm{corr}}$) is the regression-corrected value of Log ($Q_{t,\mathrm{pred}}$) and Y is the value given by the regression equation. Next, the field-derived parameter with the highest $|r|$ with the remaining residual, calculated with Log($Q_{t,\mathrm{corr}}$) replacing Log($Q_{t,\mathrm{pred}}$) in equation (14), was identified and a regression of the remaining residual against both field-derived parameters was conducted. New corrected values of Log($Q_{t,\mathrm{corr}}$) were calculated using this multiple regression. This process was repeated until little reduction of *RMSEL* was obtained with the addition of a new parameter. In addition, the single

Table 4. Representative Mass Flux Equations Used in the Total Horizontal Mass Flux Calculation

	Expression	Citation
$Q_{t,\mathrm{pred}} \propto u_*^4$	$A\frac{\rho}{g}u_*^4\left(1-\frac{u_{*t}}{u_*}\right)$	*Gillette and Passi* [1988][a]
$Q_{t,\mathrm{pred}} \propto u_*^3$	$A\frac{\rho}{g}u_*^3\left(1-\frac{u_{*t}^2}{u_*^2}\right)$	*Owen* [1964], *Shao et al*. [1993], and *Gillette and Chen* [2001]
	$A\frac{\rho}{g}u_*^3\left(1-\frac{u_{*t}^2}{u_*^2}\right)\left(1+\frac{u_{*t}}{u_*}\right)$	*Kawamura* [1951]
	$A\frac{\rho}{g}u_*^3\left(1-\frac{u_{*t}}{u_*}\right)\left(1+17.75\frac{u_{*t}}{u_*}\right)$	*Sorensen* [1991]
	$A\frac{\rho}{g}u_*^3\left(1-\frac{u_{*t}}{u_*}\right)$	*Lettau and Lettau* [1978]
$Q_{t,\mathrm{pred}} \propto u_*^2$	$A\frac{\rho}{g}u_*^2\left(1-\frac{u_{*t}^2}{u_*^2}\right)$	Modified *Shao et al*. [1993][b]

Note that the constants at the beginning of each of the original equations were replaced by a variable A that may be determined by model runs.

[a]The *Gillette and Passi* [1988] equation was originally suggested for vertical flux. However, it is included here because it is the fourth-power version of *Lettau and Lettau* [1978] and the simplest reasonable version of a fourth-power flux equation.

[b]The Shao *et al*. [1993] equation was revised to provide a relationship such that Q scales with the second power of u_*.

regression corrections using each of the two field-derived parameters with the highest $|r|$ were investigated (that is, rather than simply the sequential approach described above).

2.6. Sensitivity of Errors to Uncertainty in Site Parameters

[30] To determine the effect that uncertainty in the plot-level parameter values (u_{*t}, mean wind speed, mean scaled gap size, and vegetation cover) might have in overall model performance, a series of simulations were conducted. For all 65 sites used in this study, model predictions of horizontal flux were made, using the *Gillette and Passi* [1988] flux equation and final fitting parameters and plot-level parameters for that site. The choice of flux equation here should not impact the interpretation of these results. Wind speed distribution was estimated as a Weibull distribution [*Gillette and Passi*, 1988] with a shape parameter equal to two and mean equal to that measured at the tower closest to the site. These model predictions were set as reference values ($Q_{t,\mathrm{act}}$).

[31] Next, 100 new predictions were made ($Q_{t,\mathrm{pred}}$), drawing the values of threshold shear velocity (u_{*t}), and mean wind speed for each iteration from normal distributions with means equal to the measured value at each site and a given coefficient of variation (CV). Error (section 2.8) was calculated for the set of predictions. Values of the CV for both variables were 0.05, 0.10, 0.15, 0.20, and 0.25. All combinations of CV for both variables were used resulting in 25 (5^2) estimates of error. CV for fractional cover and mean scaled gap size was set to be 5% because they were found to not contribute significantly to the total error.

2.7. Other Models

[32] Field data were used to parameterize three additional models of the impact of vegetation upon horizontal aeolian flux: the *Marticorena et al*. [1997b] (hereafter MAR) model, the *Shao* [2008] model (hereafter SHAO), and the RWEQ [*Fryrear et al*., 1998]. Because the OK model is fundamentally a model of how vegetation impacts horizontal flux, only those portions of MAR, SHAO, and RWEQ that pertain to the effect of vegetation upon horizontal flux were implemented. That is to say, to provide the most reasonable basis of comparison, threshold shear velocity for the soil (i.e., without the effect of vegetation) in all model calculations was set to that estimated in the field. In the RWEQ and SHAO model, where there are multiple factors related to soil that were not measured, these were set to constant values to allow a consistent basis of comparison.

[33] The RWEQ, MAR, and SHAO models all have a multiplicative A term. Unlike our treatment of OK and MOK, in which we optimized on A, we accounted for this multiplicative factor for RWEQ, MAR, and SHAO in a simpler way. The A that minimizes the *RMSEL* must be the average of $\mathrm{Log}(Q_{t,\mathrm{act}})/\mathrm{Log}(Q_{t,\mathrm{pred}})$. When calculated this way, unfortunately, A is negative for the MAR and SHAO models. This is an undesirable result resulting from the fact that $Q_{t,\mathrm{pred}}$ is negatively offset from $Q_{t,\mathrm{act}}$. In order to get a more realistic view of the prediction error of these models, the values of $Q_{t,\mathrm{pred}}$ were corrected for both the slope and the intercept of the regression of $Q_{t,\mathrm{pred}}$ versus $Q_{t,\mathrm{act}}$. All RWEQ, MAR, and SHAO model results discussed hereafter are these corrected values of $Q_{t,\mathrm{pred}}$.

2.7.1. Marticorena *et al.* [1997b] Model

[34] The basic flux equation for the MAR model is

$$Q_{\mathrm{tot,pred}} = (1-F_g)A\frac{\rho}{g}\sum u_*^3 \int_{D_p}\left(1+\frac{u_{*\mathrm{tv}}}{u_*}\right)\left(1-\left(\frac{u_{*\mathrm{tv}}}{u_*}\right)^2\right)dD_p \tag{16}$$

where D_p is the particle diameter and $u_{*\mathrm{tv}}$ is the threshold shear velocity for a vegetated surface, which is given by

$$u_{*\mathrm{tv}} = \frac{u_{*t}}{f_{\mathrm{eff}}} \tag{17}$$

[35] In the model as originally published, u_{*t} is evaluated for each particle size. Here, u_{*t} is set to that measured in the field and therefore (16) simplifies to

$$Q_{t,\mathrm{pred}} = (1-F_g)A\frac{\rho}{g}\sum u_*^3\left(1+\frac{u_{*\mathrm{tv}}}{u_*}\right)\left(1-\left(\frac{u_{*\mathrm{tv}}}{u_*}\right)^2\right) \tag{18}$$

[36] For a surface with vegetation,

$$f_{\mathrm{eff}} = f_{\mathrm{eff},z_1} f_{\mathrm{eff},z_2} \tag{19}$$

where f_{eff,z_1} accounts for the roughness of the rough soil surface and f_{eff,z_2} accounts for the roughness provided by the vegetation. In the absence of vegetation, f_{eff} is calculated as f_{eff,z_1} only.

[37] f_{eff,z_1} is given by

$$f_{\mathrm{eff},z_1} = 1-\left(1n\left(\frac{z_{o,1}}{z_{\mathrm{os}}}\right)\right)\left(1n\left(0.35\left(\frac{X_1}{z_{\mathrm{os}}}\right)^{0.8}\right)\right)^{-1} \tag{20}$$

where z_{os} is the roughness length of the smooth surface [set to 10^{-5} m; *Marticorena et al*., 1997b], X_1 is the distance between soil roughness elements [set to 0.1 m; *Marticorena et al*., 1997b], and $z_{o,1}$ is the roughness length imparted by the soil roughness. $z_{o,1}$ was set to 5.38×10^{-4} m, which is consistent with lateral cover of soil roughness elements $\geq$0.11 and soil roughness elements 0.01 m in height (equation (8)).

[38] f_{eff,z_2} is given by

$$f_{\mathrm{eff},z_2} = 1-\left(1n\left(\frac{z_{o,2}}{z_{o,1}}\right)\right)\left(1n\left(0.35\left(\frac{X_2}{z_{o,1}}\right)^{0.8}\right)\right)^{-1} \tag{21}$$

where $z_{o,2}$ is the roughness length imparted by the vegetation and X_2 is one-third the distance between plants and can be calculated from our field data calculated by $(\bar{L}+0.5\bar{W})/3$.$z_{o,2}$ was calculated using equation (8).

[39] For the implementation of the MAR model here, u_* was determined using equation (7) and $z_{o,2}$ or in the absence of vegetation $z_{o,1}$.

2.7.2. Shao [2008] Model

[40] The basic flux equation for the SHAO model is

$$Q_{\mathrm{tot,pred}} = (1-F_g)A\frac{\rho}{g}\sum u_*^3 \int_{D_p}\left(1-\left(\frac{u_{*\mathrm{tv}}}{u_*}\right)^2\right)dD_p \tag{22}$$

$u_{*\mathrm{tv}}$ is given by

$$u_{*\mathrm{tv}} = \frac{u_* t}{\sqrt{(1 - m\sigma\beta)}(1 + m\beta\lambda)} \tag{23}$$

where u_{*_t} is evaluated for each particle size, m is an empirical constant ($m = 0.16$) [*Shao*, 2008, p. 307] and β is the ratio of element to surface drag coefficients ($\beta = 202$) [*Shao*, 2008 p. 307]. $\sigma = A_B/A_P$ and is given by *Shao* [2008] as a constant but can be calculated from our field data assuming cylindrical plant geometry (i.e., $A_B = \pi/4\bar{D}^2$ and $A_P = \bar{D}h$). In the original SHAO model, $u_{*\mathrm{tv}}$ also had corrections for soil moisture, salt concentration, and surface crust. Since we had direct measurements of u_{*_t}, these were not used (i.e., were set to one) nor was the dependence upon grain size used. Therefore, equation (22) simplifies to

$$Q_{t,\mathrm{pred}} = (1 - F_g)A\frac{\rho}{g}\sum u_*^3\left(1 - \left(\frac{u_{*\mathrm{tv}}}{u_*}\right)^2\right) \tag{24}$$

u_* was determined using equation (7) with z_o calculated from equation (8) using lateral cover calculated from equation (9).

2.7.3. Revised Wind Erosion Equation

[41] The RWEQ model calculates horizontal transport as it increases across an agricultural field toward maximum value. This maximum value was used here as the main point of comparison:

$$Q_{t,\mathrm{pred}} = A{\cdot}0.1098{\cdot}WF{\cdot}EF{\cdot}SCF{\cdot}K^{'}{\cdot}SLR_F{\cdot}SLR_S{\cdot}SLR_C \tag{25}$$

where WF is the weather factor ($\mathrm{g\,m^{-1}\,d^{-1}}$), EF is the erodible fraction (dimensionless), SCF is the soil crust factor (dimensionless), K' is the soil roughness factor (dimensionless), SLR_F is the soil loss ratio for flat cover (dimensionless), SLR_S is the soil loss ratio for plant silhouette (dimensionless), and SLR_C is the soil loss ratio for growing plant canopy (dimensionless). WF is given by

$$WF = 4.8 \times 10^{-2}\frac{\rho}{g}\sum_{U_2} U_2(U_2 - U_t)^2{\cdot}SW{\cdot}SD \tag{26}$$

where U_2 is the wind speed ($\mathrm{m\,s^{-1}}$) at 2 m and U_t is the threshold wind speed ($\mathrm{m\,s^{-1}}$) at 2 m. SW is a factor that corrects for soil wetness and SD is a factor that corrects for snow cover; both were set to one. The coefficient 4.8×10^{-2} includes both an empirical factor (1/500) and corrections to yield units of $\mathrm{g\,m^{-1}\,d^{-1}}$ for consistency with the other models in this application. Wind speed at 2 m was calculated using measured wind speed at height z, U_z:

$$U_2 = U_z\frac{1n(2/z_o)}{1n(z/z_o)} \tag{27}$$

where z_o was calculated using equation (8). Threshold wind speed at 2 m, U_t, was calculated as

$$U_t = \frac{u_{*t}}{K}1n\left(\frac{2}{z_o}\right) \tag{28}$$

[42] EF is a complicated function of soil texture:

$$EF = \frac{1}{100}\Big(29.09 + 0.31\%sand + 0.17\%silt + 0.33(\%sand/clay) - 0.259\%organicmatter - 0.95\%CaCO_3\Big) \tag{29}$$

[43] Texture data were not available, so the maximum possible value of EF (0.630) was calculated using the soil parameters given in *Fryrear et al.* [1998]: 0.18% organic matter, 93.6% sand, 0.5% silt, 5.9% clay, 0% $CaCO_3$. Using these same soil parameters, SCF, given by

$$SCF = \Big(1 + 0.0066(\%clay)^2 + 0.021(\%organicmatter)^2\Big)^{-1} \tag{30}$$

was calculated as 0.813, which is close to the highest value reported by *Fryrear et al.* [1998], 0.823. K' is a correction for soil random roughness, which was not measured, so it was set to its maximum value, 1.0, which corresponds to a rough soil. SLR_F corrects for the amount of flat plant residue on the surface, which we assumed to be zero because our field sites were not agricultural fields with residue and was therefore set to 1.0. SLR_S is given by

$$SLR_S = \mathrm{Exp}\big(-0.344\lambda^{0.6413}\big). \tag{31}$$

[44] SLR_C corrects for the amount of soil covered by plants, i.e., $(1 - F_g)$, and is given by

$$SLR_C = \mathrm{Exp}\big(-0.5614{F_g}^{0.7366}\big) \tag{32}$$

[45] For the RWEQ model, maximum values of soil parameters (SD, SW, EF, SCF, and K') were set as constants to obtain a consistent set of predictions for which soil conditions (except U_t) are common to all sites. Because the purpose of using additional models' horizontal flux predictions in this report is to compare how they treat vegetation with respect to how the OK model treats vegetation, the use of constant values for soil parameters is justified. This is particularly true with the RWEQ model because of the linear way in which these parameters are included in the flux equation (i.e., equation (25)).

2.8. Model Comparison and Error Metrics

[46] The *RMSEL* was utilized instead of the root mean squared error (*RMSE*, the error calculated without first taking the log) because the horizontal flux estimates spanned two orders of magnitude. The use of *RMSEL* instead of *RMSE* is justified by the purposes of this study, one of which is to estimate horizontal aeolian transport over a wide range of field conditions including those with low flux. The use of *RMSE* would emphasize errors of prediction for larger fluxes considerably more than errors of prediction for smaller fluxes because the same relative error in the both cases yields a larger error in the case of the larger flux. It is our contention that locations with higher horizontal transport are not necessarily more meaningful in terms of the total amount of transport in or dust produced from natural landscapes. This is particularly true when the potential for horizontal aeolian transport to produce atmospheric dust is

considered. The amount of dust produced from landscapes (i.e., the vertical flux in units of $\mathrm{M\,L^{-2}\,t^{-1}}$) can be approximated as a linear function of the horizontal flux with the constant of proportionality, the dust production efficiency, depending on soil characteristics [e.g., *Gillette*, 1977]. Therefore, the amount of dust produced from a landscape is the product of the horizontal flux, the area over which the horizontal flux occurs, and the dust production efficiency. That is to say, large areas with relatively low flux may produce as much dust as small areas with higher flux. With this in mind, it would seem necessary to have a model that can estimate both the small fluxes and the large fluxes equally well. Thus, we chose to use as our error metric *RMSEL*, which emphasizes error for small fluxes and large fluxes equally, over *RMSE*, which emphasizes error for large fluxes over small fluxes.

[47] An additional benefit of the use of *RMSEL* over *RMSE* is that *RMSEL* provides an estimate of relative error whereas *RMSE* provides only an estimate of absolute error. Relative error is arguably more important than absolute error when the model/measured data span two orders of magnitude, as they do here. It can be shown that 10^{RMSEL} is the geometric mean of the ratio of $Q_{t,\mathrm{pred}}$ to $Q_{t,\mathrm{act}}$. Because

$$Q_{t,\mathrm{pred}} - Q_{t,\mathrm{act}} = \varepsilon \tag{33}$$

where ε is the absolute error, the ratio of $Q_{t,\mathrm{pred}}$ to $Q_{t,\mathrm{act}}$ can be expressed as

$$\frac{Q_{t,\mathrm{pred}}}{Q_{t,\mathrm{act}}} = 1 + \frac{\varepsilon}{Q_{t,\mathrm{act}}} \tag{34}$$

where $\varepsilon/Q_{t,\mathrm{act}}$ is the relative error. 10^{RMSEL} is the geometric mean of equation (34) and thus, we propose as a metric of error, ε_r:

$$\varepsilon_r = 10^{\mathrm{RMSEL}} - 1 = \left\langle 1 + \frac{\varepsilon}{Q_{t,\mathrm{act}}} \right\rangle - 1 \tag{35}$$

[48] Although ε_r is not strictly equal to the relative error, it is an approximation of it with the property that it is equal to zero when there is no prediction error. ε_r values for the MAR, SHAO, and RWEQ models were calculated after correcting $Q_{t,\mathrm{act}}$ from these models by the slope and intercept of their regression against $Q_{t,\mathrm{act}}$.

3. Results

3.1. Characteristics of the Model Input Data and Horizontal Flux Estimates

[49] Characteristics of model input data, including vegetation, threshold shear velocity, and wind are given in Table 2 and further in Table S1, Supporting Information. Bare sites were found in both Moab and Clear Spot Flat, Utah, and the latter study site also had the largest average gap of 11 m. Average scaled gap (gap size/canopy height) ranged from 18 in the shrubland of Fivemile Mountain, Utah to 282 in the burned Clear Spot Flat, Utah sites. Threshold shear velocity for unvegetated soil fell in the range of 0.19–1.04 $\mathrm{m\,s^{-1}}$. During the experimental period, a large proportion of the wind speeds were lower than 5 $\mathrm{m\,s^{-1}}$ for all study sites, and peak wind speeds varied from 12 to over 26 $\mathrm{m\,s^{-1}}$, observed in the Owens Valley, California site (Table 5, Figure 3).

[50] The fit of $q(z)$ to equation (1) generally gave very good fits (Table S1, Supporting Information). Coefficients of determination for these fits, r^2, are not particularly useful because many of the sites had only three BSNE traps on a stem and equation (1) has three parameters, thus resulting in $r^2 = 1$. However, for sites with more than three BSNEs on a stem (i.e., all sites excluding the Utah sites), the fits are generally very good, with only two being fit with $r^2 < 0.9$. BSNE-estimated $Q_{t,\mathrm{act}}$ spanned two orders of magnitude, with the greatest flux of 98 $\mathrm{g\,m^{-1}\,d^{-1}}$ found in a site at the JER, New Mexico, where grass cover had been removed (Figure 4). $Q_{t,\mathrm{act}}$ was generally the lowest in the shrubby grassland of Owens Valley sites, despite the high wind speeds at these sites.

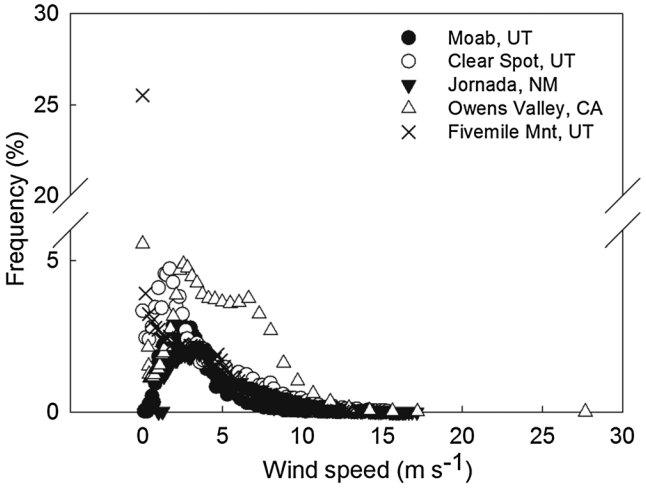

Figure 3. Frequency distribution of wind speeds used in the mass flux modeling for major study sites. More details related to the characteristics of the study sites may be found in Tables 1 and S1.

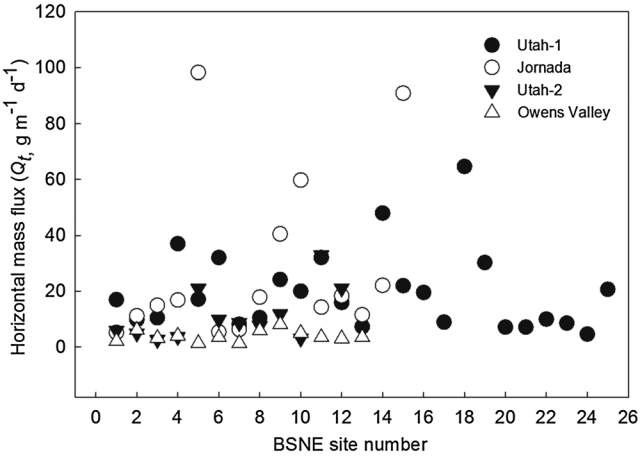

Figure 4. Horizontal mass flux ($Q_{t,\mathrm{act}}$, $\mathrm{g\,m^{-1}\,d^{-1}}$) measured by BSNEs located in the major study sites. More details of the study sites are listed in Table 1.

3.2. Model Evaluation

[51] As expected, different mass flux equations (Table 4) yielded different best-fit values of key model parameters for the OK model (Table 6). The mean optimum values for the roughness length (z_o), e-folding distance for recovery of shear stress (C), and $\left(\frac{u_{*s}}{u_*}\right)_{x=0}$ ranged 0.77–0.83, 5.6–6.2, and 0.28–0.32 m, respectively. The A constants have a variety of magnitudes due to the different forms of the mass flux equations. Uncertainties of the fits from the leave-one-out cross-validation are small relative to parameter values, indicating confidence that the fitting procedure was stable and that these are the best predicted values of these parameters.

[52] The performance of the OK model in combination with different mass flux equations was evaluated by regression of $Q_{t,\mathrm{pred}}$ against $Q_{t,\mathrm{act}}$ (Table 7). The regression equations generally had a slope close to 1 and a fairly small intercept (−0.053 to 0.058) except in the case of the modified *Shao et al*. [1993] flux equation. r^2 ranged from 0.41 to 0.45 and ε_r ranged from 2.1 to 2.4, except for the modified *Shao et al*. [1993] flux equation for which ε_r was 6.0. The *Gillette and Passi* [1988] and *Sorensen* [1991] flux equations had the best and essentially the same values of r^2 and ε_r for the OK model (Figure 5). Correction for those field-measured parameters with the highest correlation with residuals (median plant height, F_g, u_{*t}, and median wind speed) lowered ε_r to 1.0 for both flux equations (Table 8, Figure 5).

[53] The MOK model, in which z_o was allowed to vary with lateral cover and plant height, did not perform as well as the original OK model which sets z_o to a constant for all

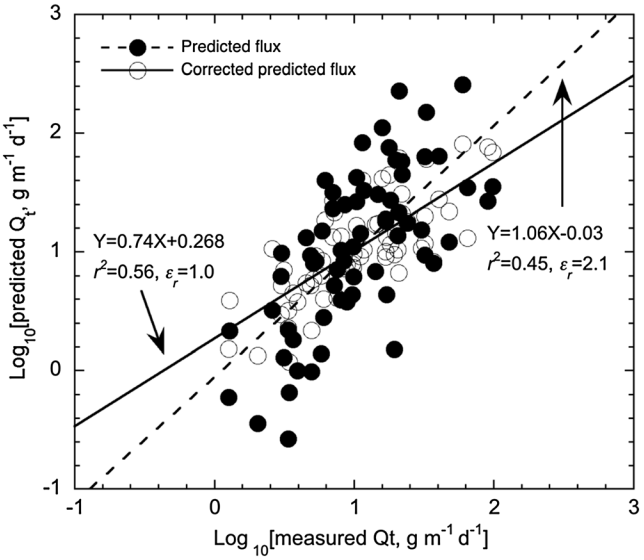

Figure 5. Comparison between OK model-estimated and BSNE-monitored horizontal aeolian fluxes at various sites in the western United States, using the *Gillette and Passi* [1988] mass flux equation. More information about basic predictions and corrected predictions may be found in Tables 7 and 8, respectively.

Table 6. Optimum Mean Values of OK and MOK Model Parameters Obtained by Leave-One-Out Cross-Validation for Different Mass Flux Equations

Mass Flux Equation	z_o(m)	A ($\times 10^{-3}$)	C	$\left(\frac{u_{*s}}{u_*}\right)_{x=0}$
OK model				
Gillette and Passi [1988]	0.077 ± 0.015	0.54 ± 0.23	5.6 ± 0.63	0.32 ± 0.072
Shao et al. [1993]	0.079 ± 0.015	26 ± 10	5.6 ± 0.89	0.29 ± 0.078
Kawamura [1951]	0.077 ± 0.015	16 ± 5.9	5.7 ± 0.75	0.31 ± 0.072
Sorensen [1991]	0.078 ± 0.015	7.3 ± 1.2	5.8 ± 0.86	0.31 ± 0.086
Lettau and Lettau [1978]	0.081 ± 0.015	39 ± 17	5.8 ± 0.93	0.30 ± 0.080
Modified *Shao et al*. [1993]	0.083 ± 0.012	780 ± 150	6.2 ± 1.0	0.28 ± 0.11
MOK model				
Gillette and Passi [1988]	—	4.3 ± 0.72	5.1 ± 0.28	0.34 ± 0.045
Shao et al. [1993]	—	180 ± 27	5.1 ± 0.24	0.33 ± 0.063
Kawamura [1951]	—	110 ± 16	5.1 ± 0.24	0.33 ± 0.073
Sorensen [1991]	—	23 ± 3.3	5.1 ± 0.28	0.33 ± 0.059
Lettau and Lettau [1978]	—	310 ± 51	5.1 ± 0.23	0.33 ± 0.073
Modified *Shao et al*. [1993]	—	880 ± 72	5.3 ± 0.52	0.33 ± 0.071

Table 7. Regression Analysis of OK and MOK Model Performance in Predicting Total Horizontal Mass Flux Based On Different Mass Flux Equations

	Slope[a]		Intercept[a,b]		r^2		ε_r	
Mass Flux Equation	OK	MOK	OK	MOK	OK	MOK	OK	MOK
Gillette and Passi [1988]	1.06	0.97	−0.053	−0.052	0.45	0.56	2.1	3.0
Shao et al. [1993]	1.03	1.04	0.019	0.026	0.41	0.57	2.3	3.3
Kawamura [1951]	1.07	1.05	0.061	0.043	0.44	0.58	2.3	3.2
Sorensen [1991]	1.05	1.05	0.058	0.041	0.45	0.58	2.1	3.2
Lettau and Lettau [1978]	1.07	1.05	0.032	0.050	0.42	0.56	2.4	3.6
Modified *Shao et al*. [1993]	1.06	1.10	−0.57	−1.29	0.41	0.56	6.0	33

[a]For regression of Log(predicted) versus Log(actual).
[b]Units of Log(g m^{-1} d^{-1}).

Table 8. Stepwise Regression Analysis and the Corrected Errors by Adding Different Factors for Horizontal Mass Flux Prediction for Both OK and MOK Models

Intercept	Plant Height (m)	Fractional Cover, F_g	u_{*t} (m s^{-1})	Median Wind Speed (m s^{-1})	r^2	ε_r
OK model						
Original					0.45	2.1
−0.41	0.024				0.53	1.4
−0.49		1.61			0.36	1.6
−0.59	0.020	0.88			0.48	1.2
−1.21	0.022	0.68	0.014		0.52	1.1
−1.97	0.020	1.15	0.015	0.0022	0.56	1.0
MOK model						
Original					0.31	3.0
−0.28	0.018				0.32	2.6
−1.32		0.028			0.29	2.1
−1.73	0.020	0.030			0.32	1.6
−1.72	0.021	0.030	−0.086		0.34	1.6
−1.71	0.021	0.030	−0.090	-1.9×10^{-5}	0.34	1.6

Calculations were based on the *Gillette and Passi* [1988] mass flux equation. Original r^2 and ε_r refer to the cross-validation values in Table 7. The empirically corrected horizontal mass flux values are given by original flux estimate + Intercept + Sum (Coefficient * Factor) for all of the factors.

data points. Values of C and $\left(\frac{u_{*s}}{u_*}\right)_{x=0}$ were close to those found with the OK model, and A varied across several orders of magnitude in much the same pattern as the OK model (Table 6). r^2 for $Q_{t,\text{pred}}$ from the MOK model with $Q_{t,\text{act}}$ were in the range 0.31–0.34 and values of ε_r were 3.0–3.6 for all flux equations except the modified *Shao et al.* [1993] equation, which had a very high ε_r of 33. In all, the *Gillette and Passi* [1988] flux equation provided the best estimates (lowest ε_r) for the MOK model (Table 7). Empirical corrections to the MOK model using this flux equation were able to reduce ε_r by about half, to 1.6 (Table 8).

[54] Results from the uncertainty analysis show that minimum expected ε_r when both u_{*t} and median wind speed are known within 5% (i.e., when CV = 0.05) is around 0.4 (Figure 6). Uncertainty in u_{*t} and mean wind speed of 25% leads to an expected ε_r ~7.

3.3. Other Models

[55] Of the other models evaluated here, only RWEQ predicted flux for all 65 sites (Table 9). The MAR model-predicted flux for only three sites (i.e., no flux was predicted for 62 sites) and the SHAO model-predicted flux for 38 sites (i.e., no flux was predicted for 27 sites). In comparison to these models, the OK model showed the highest value of r and the lowest value of ε_r, except for the MAR model. The low value of ε_r for the MAR model is somewhat misleading as this represents the error for only the sites where the MAR model predicts any flux. We believe that the failure of MAR to predict flux at the vast majority of sites constitutes a serious failure of this model.

[56] Among the models that use lateral cover to describe vegetation distribution as a control on threshold shear velocity (i.e., SHAO and MAR), SHAO predicted flux for more sites than MAR. 33 of the 38 sites at which SHAO predicts that flux had absolute value of error of the logs (i.e., $|\text{Log}(Q_{t,\text{pred}}) - \text{Log}(Q_{t,\text{act}})|$ indicating error greater than an order of magnitude (i.e., >1) (Figure 7). For OK results among these 38 sites, error was greater than an order of magnitude for only two sites. For the sites with the most positively skewed scaled gap size distributions (i.e., (mean scaled gap size)/(median scaled gap size)

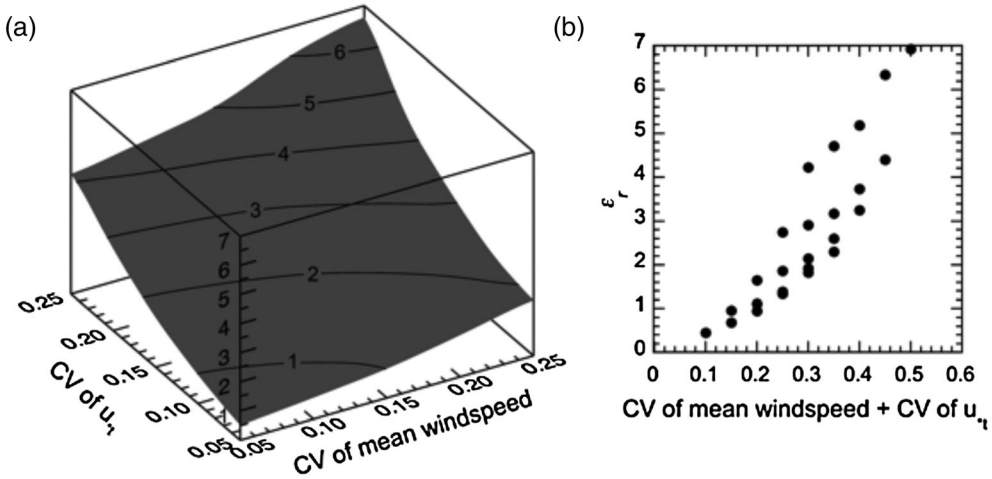

Figure 6. Expected error, plotted as ε_r, when u_{*t} and mean wind speed are uncertain. The degree of uncertainty is estimated using the coefficient of variation (CV). (a) The surface plots ε_r against CV of mean wind speed and u_{*t}. The surface has been interpolated. (b) ε_r plotted against the sum of the CVs of mean wind speed and u_{*t}.

Table 9. Summary of the Performance of OK and Other Models Compared in This Study

Model	n	r^2	ε_r
OK*	65	0.45	2.1
MOK*	65	0.35	2.8
MAR	3	0.27	0.6
SHAO	38	0.08	41
RWEQ	65	0.03	240

The OK and MOK models used the *Gillette and Passi* [1988] flux equation and the values of the best-fit parameter values from Tables 6. n is the number of sites predicted by the model with nonzero aeolian flux, r^2 is coefficient of determination between $Q_{t,\mathrm{pred}}$ and $Q_{t,\mathrm{act}}$ (r), and ε_r is relative prediction errors given by equation (35).

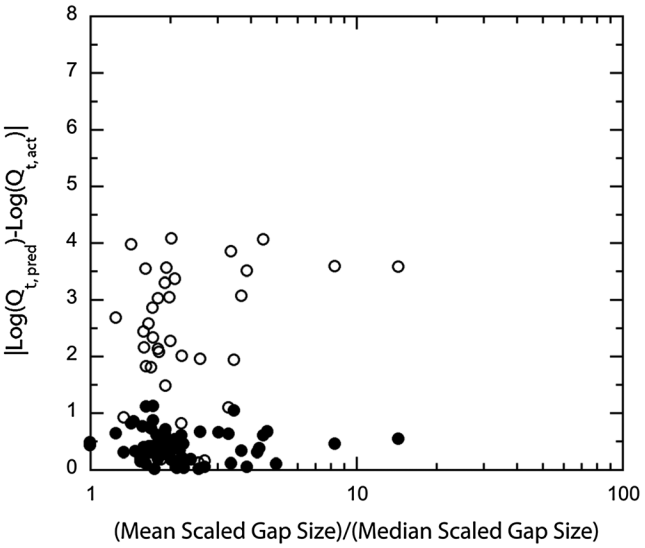

Figure 7. Error, $|\mathrm{Log}(Q_{t,\mathrm{pred}}) - \mathrm{Log}(Q_{t,\mathrm{act}})|$, plotted against a proxy for the skewness of the gap size distribution (i.e., mean scaled gap size divided by median scaled gap size). OK results are plotted as closed circles. SHAO results are plotted as open circles. Only sites ($n = 38$) for which the SHAO model predicts flux are plotted.

> 1.5, 35 sites, scaled gap size is the gap size divided by plant height), absolute value of error of the logs for SHAO predictions exceeded an order of magnitude at 28 sites. For these same positively skewed sites, absolute value of the error of the logs for the OK model exceeded an order of magnitude at only two sites. These same comparisons cannot sensibly be made for MAR because the model-predicted flux for only three of the 65 sites.

4. Discussion

[57] The present work uses a large number of sites ($n = 65$) over a wide geographic area with a variety of soil and vegetation types and with temporal periods from 4–5 months (Tables 1 and 5). The sites that were chosen for this study were all those that we could identify at the time of the research and were not established for the purposes of this project. Aeolian activity was observed at all sites, only two of which were unvegetated (Table 1). In the present study, the OK-modeled values of $Q_{t,\mathrm{pred}}$ were significantly correlated with $Q_{t,\mathrm{act}}$ at the 99% level ($r_{\mathrm{crit}} < 0.325$ [*Rohlf and Sokal*, 1981]) with approximate relative errors (ε_r) around 2–3, depending on flux equation, without empirical correction. With empirical correction, ε_r can be as low as 1.0 when all four field measures are incorporated (h, F_g, u_{*t}, and median wind speed), but the addition of just h and F_g can bring ε_r to 1.2–1.3. Although inclusion of median wind speed does improve model performance in terms of ε_r, it provides at best a small improvement. For the empirical correction, h, F_g, and u_{*t} can easily be estimated in the field, and therefore, their use for empirical correction of model estimates should be straightforward in most cases. The fact that these parameters are significantly correlated to model error suggests that future improvements to the model should involve modifications related to these parameters.

[58] The OK model, as originally conceived, treated z_o as a constant. It was thought that the z_o in the model was the roughness length due to the roughness of the soil alone. However, our estimation of model parameters shows in all cases that the best results are obtained when z_o is 0.07–0.08 m, which is the roughness length expected for vegetated surfaces rather than due to the soil roughness only. There are reliable published relationships between vegetation cover and z_o [e.g., *Marticorena et al.*, 1997b], and a modification of the OK model was evaluated to determine whether taking into account vegetation roughness in the model might improve it. Although $Q_{t,\mathrm{pred}}$ from this MOK model is still significantly correlated with $Q_{t,\mathrm{act}}$, the correlations are lower (and the relative errors, ε_r, are higher) than the original OK model. In order to obtain even these results, the relationship for z_o had to be adjusted to increase roughness (equation 12).

[59] From a modeling perspective, the fact that the surface must be treated as if it were rougher than the bare soil and also rougher than predicted from the published relationships between vegetation and z_o suggests one of the two things under the long-term field measurement scenarios; either the surface really behaves as if it is rougher than expected or u_{*t} behaves as if it is lower than expected. Because airflow over rough surfaces is better understood from theoretical considerations and laboratory experiments and is also more predictable than soil surface characteristics over extensive temporal and spatial scales, the latter explanation is more likely. This conclusion is independent of the OK or MOK treatment of vegetation. Consider, for example, two of our sites that were unvegetated. These sites experienced flux and had values of $Q_{t,\mathrm{act}}$ in the middle of our measured range. Use of typical values for z_o for bare soil (<0.01 m) did not yield any times at which u_* exceeded u_{*t} even though the estimated u_{*t} values were not particularly high ($u_{*t} = 0.48$ and $0.71\ \mathrm{m\ s^{-1}}$).

[60] Our understanding of the physics of aeolian transport requires that, on certain temporal and spatial scales, transport can only occur when u_{*t} exceeds u_*. We do not refute this. Nevertheless, over spatially extensive real landscapes in which transport is measured over a period of several months, our results suggest that u_{*t} behaves as if it is lower than what is measured at a single time period. The values of u_{*t} used here were the minimum values measured at 10-m intervals extending 50 m outward from the BSNE stems. They should, therefore, provide a reasonable estimate of the minimum threshold in the area over which saltation

flux may be expected to contribute to measured BSNE fluxes. But, these measurements were only taken at one time. Further research is required to understand how u_{*t} varies through time in natural landscapes experiencing aeolian transport. Until this discrepancy can be reconciled, our results suggest that adequate modeling results can be obtained by treating the surface as if it is rougher (i.e., greater z_o) than expected. Using a constant z_o, as in the OK model, provides a better fit to the observational data than a z_o that varies with vegetation density and height, as in the MOK model. For the sake of better predictions as well as model parsimony, the OK model should be preferred over the MOK model for the time being.

[61] Our evaluation of the OK model shows that it compares quite favorably to other studies that have evaluated models of horizontal aeolian flux quantitatively in the field. *Van Pelt et al*. [2004] compared estimates of aeolian soil loss from bare fields around Big Springs, Texas, USA, for 41 events and modeled the flux using the RWEQ. Using the same method of error evaluation used here, we calculated an ε_r of 2.9. The RWEQ users guide published by *Fryrear et al*. [1998] provided data on measured and modeled flux at 51 agricultural fields for periods of several months that were used to calibrate the model. For the sites for which transport was predicted ($n = 49$), we calculated $\varepsilon_r = 4.6$. *Buschiazzo and Zobeck* [2008] measured 26 individual events on a bare field in the Argentine Pampas and compared these measurements with model estimates using the RWEQ and the stand-alone erosion submodel of the Wind Erosion Prediction System. Both models underestimated flux by 45% and 40%, respectively. Because they did not report actual measured values in a table or easily extractable figure format, it is impossible to conduct the same type of error evaluation used here, but taking the reciprocal of the underestimations gives 2.2 and 2.5, respectively, meaning that the models were within a factor of about 2.2–2.5 from field estimates, albeit systematically. For fields with cover under conventional and no-till agriculture fields in this same study, these two models failed to predict any sediment movement for all but one event despite observations of transport for over half of the events. For the events where flux was measured, flux was nonetheless high, averaging 6500 and 5000 $\mathrm{g\,m^{-1}\,d^{-1}}$ for conventional and no-till fields, respectively. *Feng and Sharratt* [2007] measured aeolian flux from fields (average cover = 50%) on a single soil type on the Columbia Plateau for six 1-week to 2-week periods and compared these with estimates from the Wind Erosion Prediction System. The model failed to predict any soil loss for half of the periods and significantly over predicted soil loss for the other three periods. In their study, the overall r^2 between predicted and modeled soil loss was 0.49, which is not statistically significant ($\alpha = 0.95$, $r_{\mathrm{crit}} = 0.811$, $\tau_{\mathrm{crit}} = 0.867$ [*Rohlf and Sokal*, 1981]). The fact that both the Buschiazzo and *Zobeck* [2008] and *Feng and Sharratt* [2009] studies had a considerable number of cases in which no flux was predicted despite being measured, particularly in the presence of vegetation, highlights the difficulty of simulating aeolian activity in the presence of vegetation. It is critical in these comparisons to note that all of the studies referenced above were from agricultural fields, many of them were bare, and on which soil parameters could be measured in detail. All of the studies cited above except *Feng and Sharratt* [2009] were also for individual storms. Bare soil or homogenous crop plantings and single events with on-site meteorological measurements are arguably much simpler systems for modeling aeolian transport than the structurally and spatially heterogeneous rangelands used in this study. In addition, the fact that there were several cases in which aeolian activity was not modeled, even though it was observed, constitutes a significant failure of these models. There are no such cases in the present study for the OK model and we believe that these comparisons show that the OK model performs well above benchmarks set by previous studies.

[62] Using the extensive dataset collected for this study, both the OK and MOK models outperformed the MAR, SHAO, and RWEQ models. The RWEQ model, though based on physical processes that impact aeolian transport, is a largely empirical model, with the forms of equations and their constants unconstrained by the physics of aeolian transport. The form of equations (30) and (31), for instance, do not seem to be determined by any physical process, even though λ and F_g certainly are related to the processes in question. Nonetheless, the RWEQ model has a significant advantage over the MAR and SHAO models, at least as far as the dataset used here is concerned; the RWEQ model-predicted transport for all of our sites. Unfortunately, the values it predicted showed little relation to those that were measured ($\varepsilon_r = 240$).

[63] The RWEQ model does not use lateral cover to control threshold shear velocity. Among the models that do (MAR and SHAO), both failed to predict transport for many of our sites (i.e., u_{*tv} was never exceeded). Modifications to the parameterization of z_o by increasing the roughness 100-fold, to bring z_o into the same order of magnitude as for the OK and MOK models, result in predicted transport for 34 of the sites in the MAR model and 63 of the sites in the SHAO model, but r and ε_r (for the sites for which flux is predicted) for these scenarios are worse (MAR: $r^2 = 0.01$, $\varepsilon_r = 5600$; SHAO: $r^2 = 0.01$, $\varepsilon_r = 2400$). The failure to predict flux at many sites, particularly since the sites where transport was not modeled were not simply those locations with the lowest transport, suggests difficulties in their representation of the surface.

[64] The OK (and MOK) model treats the surface fundamentally differently from the MAR and SHAO models. In the OK model, horizontal flux is possible in some locations of the landscape that are exposed while other, more protected areas do not experience transport. In the MAR and SHAO models, the entire landscape is characterized by a single threshold and transport must occur everywhere at the same time or not at all. In other words, according to the OK model, vegetation alters the distribution of shear stress on the surface, whereas in the MAR and SHAO models, vegetation changes the threshold shear stress for the entire surface. Field observations [e.g., *Gillette et al*., 2006] show that flux does not have to occur on the landscape at all places during a transport event. Laboratory results from Walter *et al*. (2012a, 2012b) corroborate this finding, showing that the area undergoing transport in an array of nonerodible elements increased with increasing wind speed. In this sense, the OK model represents the physics of transport better than the MAR and SHAO models. The fact that

the OK models show better correspondence with our field data provides further support for this view of vegetation's impact on aeolian transport.

[65] As a further test of the importance on gap size distribution, we plotted the absolute value of the error of the logs for the OK and SHAO models against the ratio of the mean scaled gap size to the median scaled gap size (Figure 7). This ratio is a proxy for the skewness of the scaled gap size distribution (values >1 are positively skewed). If our argument is correct that representation of the surface as a distribution of gaps whose size controls where and when the threshold of the surface is exceeded, the OK model should predict flux well for the most skewed sites (i.e., error at least within one order of magnitude). Conversely, the SHAO model (as well as the MAR model, but this model only predicts flux at three sites so the same comparison cannot sensibly be made) uses lateral cover to represent vegetation on the surface, which carries with it the implicit assumption that gap size distribution does not matter. If the size distribution of gaps matters, this assumption implies that the skewed sites should not have greater error than the unskewed sites.

[66] The OK model does indeed predict flux well for the most skewed sites. However, among 38 of the 65 sites that SHAO predicts any flux for, it fails to predict transport within an order of magnitude at 28 sites. All of these sites are highly skewed (mean scaled gap size/median scaled gap size >1.5). This suggests strongly that incorporating explicit information about the distribution of vegetation is a superior way to represent vegetation in aeolian transport models compared to representing vegetation by a single lateral cover.

[67] In seeming contrast to these results, *Brown et al*. [2008] was a wind tunnel study that indicated that the distribution of roughness elements is not important to shear stress partitioning. However, shear stress partitioning is not horizontal flux, the topic of this paper, so these studies are not in conflict. Indeed, the original *Okin* [2008] paper showed simultaneously that the OK model represents measurements of shear stress partitioning quite well, whereas the flux calculated from the OK model did not match that calculated from models that do not take the distribution of roughness elements into account. Shear stress partitioning is a bulk property of the surface, but the initiation of aeolian transport is a point process. Thus, there is no reason that shear stress partitioning cannot be distribution independent whilst flux is distribution dependent.

[68] Imagine, for instance, an area with roughness elements and that the lateral cover of these elements is such that the threshold shear stress is not exceeded by a constant wind according to, say, a shear stress partitioning model like that of *Raupach et al*. [1993]. Next, allow that the wind shear is almost, but not quite, at threshold and therefore there is not yet any aeolian transport. Next, envision moving these roughness elements from the center of the area toward its perimeter. Since the number of roughness elements is conserved, the lateral cover is conserved and therefore the shear stress partitioning on the surface is also conserved (at least according to the *Raupach et al*. [1993] model and the results of *Brown et al*. [2008]). However, the absence of roughness elements in the middle of the area will present a large blank spot where the wind shear will exceed threshold, and therefore, transport will occur since the system as a whole was already near threshold. This brief mental experiment shows one way in which shear stress partitioning does not have to depend on roughness distribution, but flux can depend on roughness distribution.

[69] Finally, aeolian transport is a threshold-controlled process and flux is nonlinear when shear velocity exceeds the threshold. Therefore, the difference between measured and modeled values of horizontal flux is highly dependent upon errors in wind speed and threshold shear velocity. To examine the impact of uncertainty in these site-level parameters, we examined the sensitivity of our error estimates on uncertainty in mean wind speed and u_{*t}. Other parameters also carry uncertainty, but these two have the largest impact on model error. Uncertainty in u_{*t} and mean wind speed of 5% using our simulation approach gave a minimum ε_r of 0.4, whereas uncertainty at the level of 25% for both of these site-level parameters gave ε_r of ~ 7 (Figure 6a). Our validated model using both *Gillette and Passi* [1988] and *Sorensen* [1991] gave ε_r of 2.1 (uncorrected). These uncorrected ε_r values are consistent with a total uncertainty of mean wind speed and u_{*t} of ~25% to 35% (Figure 6b). The method used in this study for estimation of u_{*t} is associated with an error of about 10% [*Li et al*., 2010] and in this study, we were not able to measure u_{*t} during the entire period of flux measurement, meaning that the error in u_{*t} is likely greater than 10%. Furthermore, we were constrained to use a relatively small number of meteorological observation stations that were, in some cases, distant from the site where flux was estimated. Thus, wind speed measurements were not collocated during the time of flux estimates, likely resulting in considerable mismatch between the winds experienced by the site and the wind speed records used in the model calibration/validation. Given the uncertainty of these site-level parameters, it is highly unlikely that the model might have estimated flux with ε_r of less than 2 or 3. We therefore consider that uncertainty in wind speed and u_{*t} is contributing significantly to our model error and that $\varepsilon_r \sim 2.1$ constitutes a very good agreement between measured and modeled values.

5. Conclusions

[70] In this study, we parameterized and validated the *Okin* [2008] wind erosion model on a variety of field sites ranging from shrubby grassland in southern New Mexico to grassland and shrubland in Utah and California, including both degraded and undegraded plant communities. The model predicted the occurrence of wind erosion at each of the sites during the experimental period, which is in agreement with the field observations, with approximate relative errors of 2.1, which we consider satisfactory, particularly given constraints in knowledge of wind speed and u_{*t}. Empirical corrections were able to further improve the approximate relative error, bringing it to 1.0. The OK model also predicted flux better than a revised version and three other published models. This comparison is made both on the basis of the statistics for those sites where transport was modeled (i.e., r and ε_r) and the number of sites on which it was modeled.

[71] In the OK model, the distribution of shear stress on the surface is modified by the presence and distribution of vegetation. In the MAR and SHAO models, vegetation alters

shear stress on the surface, but this effect is only incorporated as a bulk property of the surface impacting overall surface shear stress. This difference allows the OK model to predict flux at higher vegetation covers than the MAR and SHAO models. The effect of changing the distribution of shear stress on the surface rather than merely changing the average shear stress experienced by the surface is seen in the inability of the MAR and SHAO models to predict transport for many of our sites.

[72] No modeling study can, by itself, show that one physical model is better than another, especially in systems as complex as those investigated here and as the saying goes "All models are wrong, but some are useful" [*Box and Draper*, 1987, p. 424]. However, the arguments and results that we have presented here show that the OK model not only succeeds but that the underlying reason for the success is the fundamentally different representation of the surface compared to models where the threshold for initiation of transport is represented solely by lateral cover (i.e., MAR and SHAO). To recapitulate, these arguments are as follows: (1) lateral cover models fail to predict flux at high cover despite ample evidence in our dataset and others that flux does indeed occur and (2) measurements and models of shear velocity in vegetated landscapes show that shear velocity does decrease in the lee of vegetation.

[73] Our results (i.e., lower ε_r and flux predicted at all sites) also suggest that the understanding of vegetation's impact of shear stress in the OK model is a more realistic representation of the physics involved in aeolian transport. Indeed, even when it predicts flux, the MAR model fails to predict flux well when the distribution is highly skewed whereas the OK model's predictive capacity is independent of the skewness. Of course, some aspects of our understanding of transport in real environments remain elusive. Our results indicate that the u_{*t} that leads to sediments captured in aeolian traps is in effect lower than that estimated directly, even over a relatively large area in the vicinity of the trap. This result suggests that temporal and spatial variability of u_{*t} in vegetated landscapes is likely a fruitful avenue of research for the future. In addition, the positive correlations of plant height, vegetation cover, and u_{*t} with model error suggest directions for the modification of the model. In particular, we believe that modification of the model to incorporate capture of saltating material by vegetation would improve it. There has been some theoretical work on this [e.g., *Raupach et al*., 2001] and some work in well-controlled outdoor systems [*Gillies et al*., 2006], but so far as we know, no field research in natural landscapes.

[74] A further advantage of the OK model over the alternate models is the ease with which vegetation parameters can be measured. Despite its long history, λ is extremely difficult to measure in the field. Gap size distribution, in contrast, may be obtained by a standard transect-based vegetation survey technique [e.g., *Herrick et al*., 2005]. Recent research by *Vest et al*. [2012] supports this view. Alternatively, vegetation characteristics could be obtained by an image-based technique [*Karl et al*., 2011; *McGlynn and Okin*, 2006], supplemented by knowledge of plant height. Additionally, the recent development of high-resolution terrestrial laser scanner [e.g., *Jupp et al*., 2008] or airborne lidar might make it possible to capture the distribution of unvegetated gaps and canopy height at a much higher spatial resolution, minimizing the possibility of missing wind erosion "hot spots" while using the line-intercept method.

[75] Development of the OK model was motivated by observations of aeolian processes in semiarid shrubby grasslands of the southwestern United States and it was subsequently developed for estimating wind erosion in rangeland ecosystems. However, because the model is based on shear velocity partitioning and physical principles, its use may not be limited to rangelands. Further investigation is required to implement the OK model in other ecosystems, particularly agricultural lands, where wind erosion models have existed for decades.

[76] This study shows that the OK model provides reliable flux estimates in vegetated systems. With the calibration and error analysis that was conducted here, it is now suitable for using in modeling transport in the world's drylands. In the United States, the Natural Resource Conservation Service's Natural Resource Inventory program uses vegetation monitoring protocols that provide information on gap size and vegetation height for over 10,000 points in nonfederal lands in the Western US [*Toevs et al*., 2011]. These protocols are fully consistent with the OK model. Natural Resource Inventory methods have also been recently adopted by the Bureau of Land Management for application to most federally owned rangelands in the United States. An electronic field data collection system is now available which automatically provides the gap and height information required [*Courtright and Van Zee*, 2011]. Similar data are now being collected as part of Mongolia's national monitoring system and used in a number of countries including China and Mexico. Compatible data can be collected by pastoralists using even simpler methods [*Riginos et al*., 2011]. As consistent gap size datasets are developed for other lands, the OK model could provide improved modeling of aeolian transport elsewhere. Moving beyond local or regional studies, incorporating the OK model into global models of aeolian transport may improve estimates in vegetated regions, thus improving underestimations in these regions and contributing to better modeling of changing dust emission in response to global environmental change. This step will require reliable ways to translate modeled or remotely sensed estimates of vegetation structure into scaled gap size.

[77] **Acknowledgements.** We thank Matthew Van Scoyoc and Michelle Mattocks for their assistance in collecting soil and vegetation data. We also acknowledge Frank Urban for providing wind data for some of the Utah sites. We would also like to thank the editor, the associate editor, and three anonymous reviewers for their helpful comments. This research was supported by the USDA-Agricultural Research Service, the USDA-Natural Resources Conservation Service Conservation Effects Assessment Program, the U.S. Geological Survey, the Bureau of Land Management, and NSF EAR Grants 0720218 and NASA Grant NNX10AO97G. Any use of trade names is for descriptive purposes only and does not imply endorsement by the U.S. Government.

References

Belnap, J., R. L. Reynolds, M. C. Reheis, S. L. Phillips, F. E. Urban, and H. L. Goldstein (2009), Sediment losses and gains across a gradient of livestock grazing and plant invasion in a cool, semi-arid grassland, colorado plateau, USA, *Aeolian Res.*, *1*, 27–43, doi:10.1016/j.aeolia.2009.03.001.

Bergametti, G., and D. A. Gillette (2010), Aeolian sediment fluxes measured over various plant/soil complexes in the Chihuahuan desert, *J. Geophys. Res.*, *115*, F03044, doi:10.1029/2009JF001543.

Bowker, G. E., D. A. Gillette, G. Bergametti, and B. Marticorena (2006), Modeling flow patterns in a small vegetated area in the northern Chihuahuan Desert using QUIC (Quick Urban & Industrial Complex), *Environ. Fluid Mech.*, *6*(4), 359–384.

Bradley, E. F., and P. J. Mulhearn (1983), Development of velocity and shear-stress distributions in the wake of a porous shelter fence, *J. Wind Eng. Indust. Aerodyn.*, *15*(1–3), 145–156.

Brown, S., W. G. Nickling, and J. A. Gillies (2008), A wind tunnel examination of shear stress partitioning for an assortment of surface roughness distributions, *J. Geophys. Res.*, *113*, F02S06, doi:10.1029/2007JF000790.

Buschiazzo, D. E., and T. M. Zobeck (2008), Validation of WEQ, RWEQ and WEPS wind erosion for different arable land management systems in the Argentinean pampas, *Earth Surf. Processes Landforms*, *33*, 1839–1850, doi:10.1002/esp.1738.

Courtright, E., and J. W Van Zee (2011), The database for inventory, monitoring and assessment (DIMA), *Rangelands*, *33*(4), 21–26, doi:10.2111/1551-501X-33.4.21.

Feng, G., and B. Sharratt (2007), Validation of WEPS for soil and PM10 loss from agricultural fields within the Columbia Plateau of the United States, *Earth Surf. Processes Landforms*, *32*, 743–753, doi:10.1002/esp.i434.

Feng, G., and B. Sharratt (2009), Evaluation of the SWEEP model during high wind on the Columbia Plateau, *Earth Surf. Processes Landforms*, *34*, 1461–1468, doi:10.1002/esp.1818.

Fryrear, D. W. (1986), A field dust sampler, *J. Soil Water Conserv.*, *41*, 117–120.

Fryrear, D. W., A. Saleh, J. D. Bilbro, H. M. Shomberg, J. E. Stout, and T. M. Zobeck (1998), REVISED WIND EROSION EQUATION (RWEQ), wind erosion and water conservation research unit, USDA-ARS, Southern Plains Area Cropping Systems Research Laboratory, Technical Bulletion, No.1.

Gillette, D. A. (1977), Fine particulate emissions due to wind erosion, *Trans. Am. Soc. Agric. Eng.*, *20*(5), 890–897.

Gillette, D. A., and R. Passi (1988), Modeling of dust emission caused by wind erosion, *J. Geophys. Res.*, *93*, 14,223–14,242.

Gillette, D. A., and W. A. Chen (2001), Particle production and aeolian transport from a "supply limited" source area in the Chihuahuan Desert, New Mexico, United States, *J. Geophys. Res.*, *106*, 5267–5278.

Gillette, D. A., J. E. Herrick, and G. A. Herbert (2006), Wind characteristics of mesquite streets in the Northern Chihuahuan Desert, New Mexico, USA, *Environ. Fluid Mech.*, *6*, 21–275, doi:10.1007/s10652-005-6022-7.

Gillies, J. A., W. G. Nickling, and J. King (2006), Aeolian sediment transport through large patches of roughness in the atmospheric inertial sublayer, *J. Geophys. Res.*, *111*, F02006, doi:10.1029/2005JF000434.

Griffin, D. W., V. H. Garrison, J. R. Herman, and E. A. Shinn (2001), African desert dust in the Caribbean atmosphere: microbiology and public health, *Aerobiologia*, *17*, 203–213.

Herrick, J. E., J. W. Van Zee, K. M. Havstad, L. M. Burkett, and W. G. Whitford (2005), *Monitoring Manual for Grassland, Shrubland and Savanna Ecosystems*, vol. *1*, quick start, Uni. of Arizona Press, Tucson, AZ.

Jupp, D. L. B., D. S. Culvenor, J. L. Lovell, G. J. Newnham, A. H. Strahler, and C. E. Woodcock (2008), Estimating forest LAI profiles and structural parameters using a ground-based laser called 'Echidna', *Tree Physiol.*, *29*, 171–181. doi:10.1093/treephys/tpn022.

Karl, J. W., M. C. Duniway, and T. S. Schrader (2011), A Technique for estimating rangeland canopy-gap size distributions from high-resolution digital imagery, *Rangeland Ecol. Manag.*, *65*(2), 196–207, doi:10.2111/REM-D-11-00006.1.

Kawamura, R. (1951), Study of sand movement by wind, *Hydraulic Engineering Laboratory Report HEL-2-8*, pp. 57, Univ. of California, Berkeley, Calif.

King, J., W. G. Nickling, and J. A. Gillies (2005), Representation of vegetation and other nonerodible elements in aeolian shear stress partitioning models for predicting transport threshold, *J. Geophys. Res.*, *110*, F04015, doi:10.1029/2004JF000281.

Lancaster, N., and A. Baas (1998), Influence of vegetation cover on sand transport by wind: field studies at Owens Lake, California, *Earth Surf. Processes Landforms*, *23*, 69–82.

Lettau, K., and H. H. Lettau (1978), Experimental and micro-meteorological field studies of dune migration. In *Exploring the World's Driest Climate*, edited by H. H. Lettau and K. Lettau, IES Report, 101, pp. 110–147, Univ. of Wisconsin-Madison, Institute for Environmental Studies, Madison, Wisc.

Li, J., G. S. Okin, L. Alvarez, and H. Epstein (2007), Quantitative effects of vegetation cover on wind erosion and soil nutrient loss in a desert grassland of southern New Mexico, USA, *Biogeochemistry*, *85*, 317–332, doi:10.1007/s10533-007-9142-y.

Li, J., G. S. Okin, L. Alvarez, and H. Epstein (2008), Effects of wind erosion on the spatial heterogeneity of soil nutrients in two desert grassland communities, *Biogeochemistry*, *88*, 73–88, doi:10.1007/s10533-008-9195-6.

Li, J., G. S. Okin, J. E. Herrick, J. Belnap, S. M. Munson, and M. E. Miller (2010), A simple method to estimate threshold friction velocity of wind erosion in the field, *Geophys. Res. Lett.*, *37*, L10402, doi:10.1029/2010GL043245.

Mahowald, N. M., C. S. Zender, C. Luo, D. Savoie, O. Torres, and J. del Carral (2002), Understanding the 30-year Barbados desert dust record, *J. Geophys. Res.*, *107D*(21), 4561, doi: 10.1029/2002JD002097.

Marshall, J. K. (1971), Drag measurements in roughness arrays of varying density and distribution, *Agr. Meteorol.*, *8*, 269–292.

Marticorena, B., and G. Bergametti (1995), Modeling the atmospheric dust cycle: 1. Design of a soil-derived dust emission scheme, *J. Geophys. Res.*, *100*, 16,415–16,430.

Marticorena, B., G. Bergametti, D. Gillette, and J. Belnap (1997a), Factors controlling threshold friction velocity in semiarid and arid areas of the United States, *J. Geophys. Res.*, *102*, 23,277–23,287.

Marticorena, B., G. Bergametti, B. Aumont, Y. Callot, and M. Legrand (1997b), Modeling the atmospheric dust cycle: 2. Simulation of Saharan sources, *J. Geophys. Res.*, *102*, 4387–4404.

McGlynn, I. O., and G. S. Okin (2006), Characterization of shrub distribution using high spatial resolution remote sensing: ecosystem implication for a former Chihuahuan Desert Grassland, *Remote Sens. Environ.*, *101*(4), 554–566, doi:10.1016/j.rse.2006.01.016.

Miller, M. E., M. A. Bowker, R. L. Reynolds, and H. L. Goldstein (2012), Post-fire land treatments and wind erosion – Lessons from the MilfordFlat Fire, UT, USA, *Aeolian Res.*, *7*, 29–44, doi:10.1016/j.aeolia.2012.04.001.

Minvielle, F., B. Marticorena, D. A. Gillette, R. E. Lawson, R. Thompson, and G. Bergametti (2003), Relationship between the aerodynamic roughness length and the roughness density in cases of low roughness density, *Environ. Fluid Mech.*, *3*(3), 249–267.

Okin, G. S. (2008), A new model of wind erosion in the presence of vegetation, *J. Geophys. Res.*, *113*, F02S10, doi: 10.1029/2007JF000758.

Okin, G. S., and D. A. Gillette (2001), Distribution of vegetation in wind-dominated landscapes: implications for wind erosion modeling and landscape processes, *J. Geophys. Res.*, *106*, 9673–9683.

Owen, P. R. (1964), Saltation of uniform sand grains in air, *J. Fluid Mech.*, *20*, 225–242.

Painter, T. H., A. P. Barrett, C. C. Landry, J. C. Neff, M. P. Cassidy, C. R. Lawrence, K. E. McBride, and G. L. Farmer (2007), Impact of disturbed desert soils on duration of mountain snow cover, *Geophys. Res. Lett.*, *34*, L12502, doi:10.1029/2007GL030284.

Painter, T. H., J. Deems, J. Belnap, A. Hamlet, C. C. Landry, and B. Udall (2010), Response of Colorado River runoff to dust radiative forcing in snow, *Proc. Natl. Acad. Sci. U. S. A.*, *107*, 17,125–17,130, doi:10.1073/pnas.0913139107.

Raupach, M. R, D. A. Gillette, and J. F. Leys (1993), The effect of roughness elements on wind erosion threshold, *J. Geophys. Res.*, *98*, 3023–3029.

Raupach, M. R. (1992), Drag and drag partition on rough surfaces, *Boundary Meteorol.*, *60*, 375–395.

Raupach, M. R., N. Woods, G. Dorr, J. F. Leys, and H. A. Cleugh (2001), The entrapment of particles by windbreaks, *Atmos. Environ.*, *35*(20), 3373–3383.

Reynolds, J., and D. M. Stafford Smith (Eds.) (2002), *Global Desertification: Do Humans Cause Deserts?*, pp. 437, Dahlem University Press, Berlin.

Reynolds, R., J. Belnap, M. Reheis, P. Lamothe, and F. Luiszer (2001), Aeolian dust in Colorado Plateau soils: nutrient inputs and recent change in source, *Proc. Natl. Acad. Sci. U. S. A.*, *98*, 7123–7127, doi:10.1073/pnas.121094298.

Riginos, C., J. E. Herrick, S. R. Sundaresan, C. Farley, and J. Belnap (2011), A simple graphical approach to quantitative monitoring of rangelands, *Rangelands*, *33*(4), 6–13, doi:10.2111/1551-501X-33.4.6.

Rohlf, F. J. and R. R. Sokal (1981), *Statistical Tables*, 2ed. W.H. Freeman and Company, New York.

Seager, R., et al. (2007), Model projections of an imminent transition to a more arid climate in southwestern North America, *Science*, *316*, 1181–1184, doi:10.1126/science.1139601.

Shao, Y. (2008), *Physics and Modeling of Wind Erosion*, 2ed. Springer, New York.

Shao, Y., and M. R. Raupach (1992), The overshoot and equilibration of saltation, *J. Geophys. Res.*, *97*, 20,559–20,564.

Shao, Y., M. R. Raupach, and P. A. Findlater (1993), The effects of saltation bombardment on the entrainment of dust by wind, *J. Geophys. Res.*, *98*, 12,719–12,726.

Sokolik, I. N., and O. B. Toon (1996), Direct radiative forcing by anthropogenic airborne mineral aerosols, *Nature*, *381*, 681–683.

Sorensen, M. (1991), An analytical model of windblown sand transport, In *Aeolian Grain Transport: Mechanics*, edited by O. E. Barndorff-Nielsen and B. B. Willetts, Acta Mechanica Supplement *1*, 67–81.

Tegen, I., S. P. Harrison, K. Kohfeld, I. C. Prentice, M. Coe, and M. Heimann (2002), Impact of vegetation and preferential source areas on global dust aerosol: results from a model study, *J. Geophys. Res.*, *107*, 4576, doi:10.1029/2001JD000963.

Thomas, D. S. G., M. Knight, and G. F. S. Wiggs (2005), Remobilization of southern African desert dune systems by twenty-first century global warming, *Nature*, *435*, 1218–1221, doi:10.1038/nature03717.

Toevs, G. R., J. W. Karl, J. J. Taylor, C. S. Spurrier, M. Karl, M. R. Bobo, and J. E. Herrick (2011), Consistent indicators and methods and a scalable sampling design to meet assessment, inventory, and monitoring information needs across scales, *Rangelands*, *33*(4), 14–20, doi:10.2111/1551-501X-33.4.14.

Van Pelt, R. S., T. M. Zobeck, K. N. Potter, J. E. Stout, and T. W. Popham (2004), Validation of the wind erosion stochastic simulator (wess) and the Revised Wind Erosion Equation (RWEQ) for single events, *Environ. Modell. Softw.*, *19*, 191–198.

Vest, K., A. J. Elmore, J. M. Kaste, G. S. Okin, and J. Li (2012), Estimating total horizontal aeolian flux within shrub-invaded groundwater dependent meadows using empirical and mechanistic models, *J. Geophys. Res.*, *Revision submitted*.

Walter, B., C. Gromke, K. Leonard, C. Manes, and M. Lehning (2012a), Spatio-temporal surface shear stress variability in live plant canopies and cube arrays, *Boundary Lay. Meteorol.*, *143*, 337–356, doi:10.1007/s10546-011-9690-5.

Walter, B., C. Gromke, and M. Lehning (2012b), Shear stress partitioning in live plant canopies and modifications of Raupach's model, *Boundary Lay. Meteorol*, *144*, 217–241, doi:10.1007/s10546-012-9719-4.

Zender, C. S., H. Bian, and D. Newman (2003), The mineral dust entrainment and deposition (DEAD) model: description and 1990s dust climatology, *J. Geophys. Res.*, *108* (D4), 4416, doi:10.1029/2002JD002775.